Serial No. N7632 NAFO SCR Doc. 25/009

SCIENTIFIC COUNCIL MEETING –JUNE 2025

An approach for assessing potential climate change impacts on stock assessment and management advice with application to NAFO 3M Cod and 3NO Witch Flounder

Samuel D. N. Johnson, Beau Doherty, Scarlett Wang, and Sean P. Cox

Landmark Fisheries Research

213-2414 St Johns Street

Port Moody, British Columbia, V3H 2B1, Canada

JOHNSON, S., DOHERTY, B., WANG, S., & COX, S. 2025. An approach for assessing potential climate change impacts on stock assessment and management advice with application to NAFO 3M Cod and 3NO Witch Flounder**.** *NAFO Scientific Council Research Document*, SCR Doc. 25/009: 1-60.

Abstract

This paper demonstrates an approach to evaluating potential climate change impacts in stock assessment and management advice for Northwest Atlantic Fisheries Organization (NAFO) stocks. We reviewed and identified environmental indices that show correlation with stock productivity, represented by annual recruitment or biomass process error terms from fishery stock assessment models. Selected indices were then included as covariates to partially account for process error variability estimated in stock assessment models and in model projections. The approach was applied to NAFO 3M Atlantic Cod (*Gadus morhua*) and 3NO Witch Flounder (*Glyptocephalus cynoglossus*). Covariates used for cod included copepod abundance and a 1-year lagged spring bloom timing, where increased copepod abundance and earlier spring bloom timing were associated with higher recruitment. For Witch Flounder, selected covariates were spring bloom timing (3-year lag) and sea ice cover (8-year lag), where later spring bloom timing and increased sea ice cover were positively associated with biomass process errors. Environmental indices incorporated into stock assessment models accounted for 21% to 40% and 86% to 96% of the total variance in process errors for Atlantic Cod and Witch Flounder, respectively, although covariates inflated the total process variance for Witch Flounder. Stock assessment models with and without environmental covariates were projected 30 years to estimate stock responses to no fishing, recent 'status-quo' fishing pressure levels, and estimated limit reference fishing pressure. Indices were projected under three scenarios where they either stayed around the historical average or increased/decreased by 20% from the historical average. Model projections accounting for environmental effects show that under the estimated environmental effects, changes in covariates translate linearly to changes in recruitment or production; however, a lack of projection models means that projection scenarios are somewhat artificial and should be improved for providing real management advice. We recommend five future steps for considering climate change impacts in management advice, providing a roadmap to guide future research planning.

Table of Contents

1. Introduction

The effects of anthropogenic climate change present new uncertainties for stock assessment and management of the world's fisheries. Catch limits are often based on estimates of stock biomass and productivity, which are derived from fishery stock assessment models fit to historical data. The majority of stock assessment models assume that model parameters are stationary (i.e., constant, or varying around a constant average), but climate change is likely causing that assumption to break down (Karp et al. 2019; André E. Punt et al. 2021). For many stocks, productivity - a combination of several factors including growth, survival, recruitment, and habitat suitability - is likely affected by changing climate, ocean, and ecosystem conditions. For example, the recruitment success of cold-water species such as Atlantic Cod (*Gadus morhua*) has been linked to changes in water temperature, with higher temperatures linked to reduced reproductive success (Hare et al. 2016). Shifts such as these in fish stock productivity can increase the risk of overfishing, particularly under typical stock assessment methods that assume future productivity regimes are the same as the past.

The extent of climate change impacts on the productivity of fisheries is difficult to isolate, and a model selection approach is required. There are many environmental conditions affected by climate change, and many possible pathways for environmental conditions to affect fish productivity. Additionally, there are a variety of approaches for incorporating environmental effects into fishery stock assessment models. Changing environmental conditions can affect stock assessment model estimates of productivity and biomass in many ways, including growth rates (André E. Punt et al. 2021; Holsman et al. 2016), survival (André E. Punt, Dalton, and Foy 2020; Spencer et al. 2016), spatial distribution (Malick, Siedlecki, et al. 2020; Spencer et al. 2016), maturity (Khalsa et al. 2023), and recruitment (M. Haltuch et al. 2019; André E. Punt et al. 2021; M. A. Haltuch et al. 2020; Tolimieri et al. 2018). As such, determining the link between climate change and stock productivity often involves testing multiple competing hypotheses and/or scenario analyses.

This paper demonstrates one approach for linking selected environmental indices to productivity in fishery stock assessments for Northwest Atlantic Fisheries Organization (NAFO) stocks. We use two case studies, an age-structured model for 3M Atlantic Cod (Garrido, González-Troncoso, and González-Costas 2024), and a logistic surplus production model for 3NO Witch Flounder (*Glyptocephalus cynoglossus*) (Maddock Parsons, Skanes, and Rideout 2024). The cases represent a range of model complexities, biomass and productivity trends, and recent stock status. Moreover, both stocks likely have moderate to high overall climate vulnerability, based on a vulnerability assessment of the same species in US waters (Hare et al. 2016). Environmental indices were chosen based on their suitability as covariates for process error terms, which drive recruitment variation in 3M Cod and changes in biomass production in 3NO Witch Flounder.

In this paper, we complete the following key tasks:

1. Identify environmental variables that best account for yearly variability in recruitment for 3M Atlantic Cod and production in 3NO Witch Flounder models.

2. Demonstrate methods for incorporating selected environmental variables into current stock assessments for both species, to consider how estimates of life history parameters, stock status, and management related parameters (e.g., reference points) change when environmental covariates are included.

3. Project original and modified stock assessment models incorporating environmental covariates to compare stock responses to fishing.

4. Identify additional approaches or tools to support NAFO considering climate change impacts within Scientific Council and Commission's decision-making process.

Tasks 1 - 3 are described in the methods, results, and discussion sections of this paper, while Task 4 is covered in the discussion only. Results from tasks 1-3 provide insights on how future fish stock productivity and responses to fishing may be affected by future environmental trends and climate change impacts.

2. Methods

This section describes the approach used to incorporate environmental index data into stock assessments and projections for 3M Cod and 3NO Witch Flounder. First, we describe the annual process errors that model recruitment variability for Cod, or variability in annual biomass production for Witch Flounder. We then describe the sources of environmental data that are included in the analysis and how indices were produced from those data for each stock area. Next, we use linear modeling and a correlation analysis to select two environmental indices for each stock to use as covariates of process error terms in stock assessments. Finally, we describe how environmental indices are incorporated into the Cod and Witch Flounder stock assessment models and projections.

2.1. Indicators of Stock Productivity

2.1.1. Characterizing Atlantic Cod Population Dynamics

The NAFO division 3M stock of Atlantic Cod was assessed via a Bayesian statistical catch-at-age stock assessment model (Garrido, González-Troncoso, and González-Costas 2024). Assessments were fit to multiple data series including yearly total commercial catch, survey biomass indices, and commercial catch-at-age data (derived via an age-length key from commercial catch-at-length frequencies).

Statistical catch-at-age models are driven by recruitment. Each year, recruits are added to the population and subsequently grow, mature, and die via natural or fishing mortality. For 3M cod, annual age-1 recruitment was modeled via an average recruitment assumption, where recruitment R_t is independent of spawning biomass and follows a log-Normal distribution around an assumed mean value $\bar{R} = 45$ million fish. Yearly recruitments are estimated as

$$R_t = \bar{R} \cdot e^{\eta_t},$$

where η_t sare recruitment process errors, representing variation in cod survival from eggs released by spawners through the larval stage to become age-1 recruits.

2.1.2. Characterizing Witch Flounder Population Dynamics

The 3NO Witch Flounder stock was assessed via a state-space surplus production stock model in which population dynamics are represented by changes in an aggregate biomass in response to fishing, with changes tracked by one or more indices from surveys and fisheries (Maddock Parsons, Skanes, and Rideout 2024; Andre E. Punt 2003). The 3NO Witch Flounder model is fit to four trawl research vessel survey indices that track biomass of recruited fish 30+ cm in length, and a total commercial catch aggregated over multiple nations (Maddock Parsons, Skanes, and Rideout 2024).

Biomass dynamics in a surplus production model follow a logistic production relationship that combines recruitment, growth, and natural mortality into a single term (Schaefer 1957; Andre E. Punt 2003). Production is a function of the biomass relative to carrying capacity or unfished biomass K of the stock and the intrinsic rate of growth r, which is the stock's productivity at low stock sizes. A Schaefer production relationship is symmetric, with zero production at 100% or 0% of unfished, and maximum sustainable yield (MSY) at 50% of unfished. Yearly changes in biomass are modeled as

$$B_{t+1} = \left(B_t + r \cdot B_t \left(1 - \frac{B_t}{K}\right) - C_t\right) e^{\eta_t},$$

where B_t is the biomass at time t, and η_t is the log-Normal process error. Each year, the biomass is updated by adding production $P_t = r \cdot B_t \left(1 - \frac{B_t}{K}\right)$ to the previous year's biomass, subtracting catch, and then modifying the result by a log-normally distributed process deviation η_t. Process errors represent anomalies in the expected production relationship and are the accumulation of several years of variation in recruitment, growth, and survival (André E. Punt et al. 2021).

An initial evaluation of the process errors from the current assessment model revealed that they were unsuitable for the analysis in this paper because they had almost no variation in all years except for 2014 - 2016 (Maddock Parsons, Skanes, and Rideout 2024), so any estimated correlation would have been biased . The specification of the model in winBUGS also led to long run times, which was too long for the runs needed in this study.

We sped up the analysis by developing a faster, more efficient state-space surplus production model (SSPM) for Witch Flounder (Appendix A) implemented in Template Model Builder (Kristensen et al. 2016). In the TMB model, we specified the same prior structure as the original model, including log-Normal priors on intrinsic growth rate r and carrying capacity K, and Γ priors on biomass survey index residual variance and catchability.

The K and r priors are specified in terms of mean and precision τ, as used by WinBUGS, where precision is the inverse of the variance V, i.e.,

$$\tau = \frac{1}{V}.$$

The log-Normal r prior uses mean $\mu_r = 0.17$ and precision $\tau_r = 3.252$ based on the 4RST Witch Flounder assessment (D. Swain et al. 2012), while the carrying capacity uses mean $\mu_K = 95.8$ kt and precision $\tau_K = 11.6$ (Maddock Parsons, Skanes, and Rideout 2024).

The main difference between assumptions for the TMB and WinBugs Witch Flounder assessment model was initialising the stock as unfished (i.e., at carrying capacity K) in 1960. When initialised at a fished level, the TMB version did not converge given that there was no index data before 1984. It may be that the prior on inital biomass in the WinBugs model has a very strong influence on the estimate.

The results in this paper use maximum posterior density estimates from the TMB model. Preliminary models attempted to produce Bayes posteriors via Hamiltonian Monte Carlo via tmbstan (Monnahan and Kristensen 2018), but posterior distributions were not acceptable due to a small number of divergent transitions (Monnahan 2024).

2.2. Environmental Indices

Three environmental data sets were considered:

1. Spatial (~ 100 km resolution for North Atlantic) monthly Sea Surface Temperature (SST) from the sixth phase of the Coupled Model Intercomparison Project (CMIP6) (Wang et al. 2023)

2. Temperature and plankton indices for the Flemish Cap (NAFO division 3M) and Grand Banks (NAFO divisions 3LNO) developed for the NAFO Standing Committee on Fisheries Environment (STACFIS) (Fréderic Cyr and Bélanger 2024)

3. Annual Newfoundland and Labrador (NL) climate indices (Frédéric Cyr and Galbraith 2020a, 2020b)

We generated CMIP6 SST indices using the CNRM-CM6-1 system model, which had the best overall performance for SST in Gulf of Maine and Scotian Shelf for 1950-2014 (Wang et al. 2023). For each stock we defined a habitat area over which to calculate SST indices with depths of 100 m - 500 m for 3M Atlantic Cod and 50 m - 1500 m for 3NO Witch Flounder [Figure 7.1; Garrido, González-Troncoso, and González-Costas (2024); Maddock Parsons, Skanes, and Rideout (2024)]. Monthly SST was then averaged across CMIP6 grid cells within the depth ranges for each stock. Bathymetry data was obtained from the General Bathymetric Chart of the Oceans (GEBCO, GEBCO Compilation Group 2024). Since the historical CMIP6 data only extended to 2014, we used model projections to extend the time series from 2015-2023, using an average of two shared socio-economic pathway scenarios (ssp245, ssp370) (Wang et al. 2023). The resulting SST indices were:

- *sst3M_high*: maximum monthly SST in each year in the Atlantic Cod habitat area in 3M.
- *sst3M_low*: minimum monthly SST in each year in the Atlantic Cod habitat area in 3M.
- *sst3M_mean*: mean monthly SST in each year in the Atlantic Cod habitat area in 3M.
- *sst3NO_high*: maximum monthly SST in each year in the Witch Flounder habitat area in 3NO.
- *sst3NO_low*: minimum monthly SST in each year in the Witch Flounder habitat area in 3NO.
- *sst3NO_mean*: mean monthly SST in each year in the Witch Flounder habitat area in 3NO.

We used the following indices from STACFIS (Fréderic Cyr and Bélanger 2024) for spring phytoplankton blooms, zooplankton, and temperature indices:

- *spring_bloom_timing3M*: spring phytoplankton bloom timing index in Flemish Pass and Flemish Cap
- *spring_bloom_intensity3M*: spring phytoplankton bloom intensity index in Flemish Pass and Flemish Cap
- *spring_bloom_timing3LNO*: spring phytoplankton bloom timing index for Northern Grand Banks and Southeast Shoal
- *spring_bloom_intensity3LNO*: spring phytoplankton bloom intensity index for Northern Grand Banks and Southeast Shoal
- *copepod_abundance3M*: copepod abundance index for Flemish Cap
- *zooplankton_biomass3M*: zooplankton biomass index for Flemish Cap
- *copepod_abundance3LNO*: copepod abundance index for 3L portion of the Flemish Cap and Southeastern Grand Bank
- *zooplankton_biomass3LNO*: zooplankton biomass index for 3L portion of the Flemish Cap and Southeastern Grand Bank
- *composite_climate3M*: An average of 3 temperature anomaly time series, including SST in 3M, mean temperature for offshore Flemish Cap, and summer mean bottom temperature for Flemish Cap.
- *composite_climate3LNO*: An average of 12 temperature anomaly time series, including SST (3L, 3N, 3O) , vertically average ocean temperature (0-176 m), cold intermediate layer volumes (Seal Island, Bonavista, inshore Flemish Cap), and mean bottom temperature in 3LNO (spring, fall)

The NL climate index described the environmental conditions on the NL shelf and in the Northwest Atlantic as a whole, as well as individual subindices of the NL climate index. Each subindex was normalized using the 1991-2020 climatological period.

The annual NL climate indices (Frédéric Cyr and Galbraith 2020a, 2020b) included 10 normalized anomalies and a composite index, which are described in Frédéric Cyr and Galbraith (2020b) as:

- *Wint.NAO*: "Average North Atlantic Oscillation over the months of December to March"
- *Air.Temp*: "Mean normalized anomalies for air temperature at Nuuk (Greenland), Iqaluit (Baffin Island), Cartwright (Labrador), Bonavista (Newfoundland) and St. John's (Newfoundland)"
- *Sea.Ice*: "Mean normalized anomalies of sea ice maximum area and season duration for Northern Labrador, Southern Labrador and Newfoundland shelves"
- *Icebergs*: "Normalized anomalies of the number of icebergs crossing 48degN on the Grand Banks"
- *SST*: "Mean normalized anomalies of Sea Surface Temperature over NAFO divisions 2HJ3KLNOP"
- *S27.T*: "Normalized anomalies of the vertically-averaged temperature at Station 27"
- *S27.S*: "Normalized anomalies of the vertically-averaged salinity at Station 27"
- *S27.CIL*: "Normalized anomalies of the summer (June-August) cold intermediate layer core temperature at Station 27"
- *CIL.area*: "Mean normalized anomalies of the summer cold intermediate layer area over hydrographic sections Seal Island, Bonavista and Flemish Cap on the Newfoundland and Labrador shelf"

- *Bottom.T*: "Mean normalized anomalies of the bottom temperature during spring (NAFO divisions 3LNOPs) and fall (NAFO divisions 2HJ3KLNO)"
- *Climate.index*: arithmetic average of all 10 NL indices above

Annual time series for all environmental indices are shown in Figures 7.2 - 7.3.

2.3. Correlation Analyses

We calculated Pearson correlation coefficients between the relevant environmental indices for each stock with recruitment process errors for Atlantic Cod and biomass process errors for Witch Flounder. Correlations among process errors and indices were evaluated, including indices with 1-2 year lags for Atlantic Cod and 1-10 year lags for Witch Flounder. The indices that resulted in the strongest correlations were then selected as covariates for linear models to determine which indices accounted for the most variability in stock productivity.

2.4. Environmental Covariates In Stock Assessments

We identified two environmental indices for each stock to incorporate into stock assessment estimation of biomass process errors η_t via

$$\eta_t = \alpha \cdot E_t + \omega_t,$$

where α is the estimated coefficient for the environmental index E_t and $\omega_t \sim N(0, \sigma_X)$ is the residual 'random component' of the yearly process error not accounted for by the environmental indices. The standard error σ_X of the random component differed by species, as indexed by X. For Cod, σ_{Cod} was estimated using the same approach as the current assessment model, while for Witch Flounder σ_{Witch} was fixed at 0.05 for estimation, and the effective standard error was estimated from the process errors for interpretation and projections (see below). The coefficients of the environmental covariates followed a normal prior, i.e., $\alpha \sim N(0, s_X)$. Standard deviation s_X differed by species, with $s_{Cod} = 1$ and $s_{Witch} = 0.03$; Normal standard deviations for both species were chosen to promote model convergence partially by trial and error, with search ranges focused on a similar scale to the standard error σ_X of the random component ω_t, given that the indices used for covariates were standarised.

For each model including covariates, we estimated the proportion of process error variance accounted for explained (R^2) by the environmental index, defined as

$$R^2 = 1 - \frac{\hat{\sigma}^2}{Var\left(\eta_{t|E_t \neq 0}\right)},$$

where $\hat{\sigma}$ is the effective standard error of the random component ω_t and $Var\left(\eta_{t|E_t \neq 0}\right)$ is the variance of the total process error term, both calculated over years the environmental index E_t exists.

2.5. Future Projections

Population models for both stocks were projected 30 years from the end of their model history in 2023. In total, there were 42 projection models, comprising three fishing levels for each of the base model and the two environmental covariate models, with three future trends in each covariate.

2.5.1. Harvest levels

All projections assumed one of three constant future fishing pressure levels, ranging from no fishing to the limit of the Removal Reference point. For Atlantic Cod, fishing pressure was simulated via the instantaneous fishing mortality rate F, with levels (i) $F_0 = 0$ for no fishing, (ii) $F_{squo} = \bar{F}_{2021:2023} \approx 0.042$ for 'status quo', which is the mean F from 2021-2023 and differs slightly for EV index models, and (iii) $F_{lim} = 0.15$ (Garrido, González-Troncoso, and González-Costas 2024). All F values given above were posterior means. Parameter uncertainty in F values was incorporated into projections.

For Witch Flounder, similar levels are used but are applied as harvest rates given that the model estimates biomass and not abundance-at-age. The three harvest levels used for projections are (i) $U_0 = 0$ (no fishing), $U_{squo} = U_{2023} \approx 0.009$ (final year harvest rate, differs by EV model), and (iii) $U_{lim} = U_{MSY} = 0.063$ (Maddock Parsons, Skanes, and Rideout 2024).

2.5.2. Environmental index projection scenarios

The CMIP6 SST indices use the mean of ssp245 and ssp370 projection scenarios for 2015-2059 (Figure 7.4). The other environmental indices considered (Frédéric Cyr and Galbraith 2020a; Fréderic Cyr and Bélanger 2024) are based on observed data and do not have model projections for future years. We therefore consider low (20% down from historical average), medium (no trend), and high (20% higher than historical average) scenarios for the observed environmental covariates incorporated into assessment models.

Environmental indices without a model are projected using an auto-correlated random walk,

$$E_{t+1} = \gamma E_t + (1-\gamma)\delta_t + \nu,$$

where γ is the estimated lag-1 autocorrelation in the index during the model's historical period, $\delta_t \sim N(0, \upsilon)$ is a random jump with standard error υ estimated from jumps in the index history, and ν produces a trend. For the high scenario, $\nu = 0.2/30$ so that indices end 20% higher than the historical average, for the medium scenario $\nu = 0$ so indices vary around the historical average, and for the low scenario $\nu = -0.2/30$ so indices end 20% below the historical average.

3. Results

3.1. Atlantic Cod

3.1.1. Environmental Covariates

Atlantic Cod recruitment deviations had the strongest correlations for copepod abundance ($\rho = 0.48$) and zooplankton biomass ($\rho = 0.33$) (Figures 7.5 and 7.6). Sea surface temperature (CMIP6), spring bloom anomalies, composite climate, and NL climate indices were not strongly correlated with recruitment deviations.

We also calculated lagged correlation among recruitment deviations and environmental variables (Table 6.1). Recruitment deviations tended to be higher when the previous year's spring bloom timing index was lower ($\rho = -0.65$) and when the maximum monthly SST was higher in two-years ($\rho = -0.4$).

We further narrowed the set of environmental indices by fitting linear models between them and recruitment process errors (Figure 7.7). Indices included copepod abundance (no lag), spring bloom timing index (1-year lag), and maximum monthly SST (2-year lag). We excluded the zooplankton biomass index from this step as it was moderately collinear with the copepod abundance index ($\rho = 0.55$, 7.5). Copepod abundance ($R^2 = 0.23$) and spring bloom timing at lag-1 ($R^2 = 0.44$) accounted for the most variation in recruitment deviation and were selected as covariates to include in the assessment model (Figure 7.7).

3.1.2. Model fits with and without environmental covariates

There were neglgible differences between model fits with and without environmental covariates (Table 6.3, Figure 7.11). Both models produce qualitatively identical results with little differences between biomass and recruitment time series. The main difference is that the recruitment process errors are split into an environmental effect component that is accounted for by the covariate and a random component for the recruitment deviation. Overall, the variance of the random process error component ω_t is reduced when an environmental covariate is included. The proportion of variance accounted for by ω_t is 21% for the copepod abundance model and 39% for the spring bloom timing model (Table 6.3, $\hat{\sigma}$). The estimated environmental covariate effects have similar magnitude, but opposite sign (Table 6.3, α).

3.1.3. Projections with and without environmental indices

In 3M Cod projections, the effect of environmental indices on stock productivity depended on a combination of the trend in the assumed environmental index and the estimated effect (i.e., α).

Copepod abundance models

Assuming that copepod abundance in the future matches the historical average leads to outcomes that are similar to the base model (Figure 7.14). In general, biomass, recruitment, and catch under the copepod abundance model are 2.5% - 10% higher than same values under the base model (Table 6.4. Increases in biomass and recruitment over the base model were related to the lower $\hat{\sigma}$ value for recruitment process errors (Table 6.3). Smaller process variation meant that log-Normal bias correction factors were smaller. While this shouldn't affect the average a great deal, bias correction factors were estimated by replicate so differences in parameter uncertainty among models is a factor.

Increasing copepod trend

If copepod abundance increased by 20% over the next 30 years, mean recruitment increases by about 10% over the zero-trend model (Table 6.4, 20% higher, $\bar{R}_{2024:2053}$). In the final year recruitment was about 20% higher, which is consistent with the increase in copepod abundance, and spawning biomass was about 14% - 18% higher than the base and zero-trend models (Table 6.4, 20% higher). Higher productivity is apparent about 4 years into the projections, as the larger year classes mature into the spawning biomass, which diverges more quickly from the base model around 2028 (Figure 8.5). Finally, as copepod abundance increased, mean catch increased by 5% over the entire projection under both the status quo and limit fishing mortality rates.

Decreasing copepod trend

When copepod abundance decreased by about 20% over the next 30 years, biomass, recruitment and catch also went down, as expected (Figure 8.6). Given the model structure, a declining copepod abundance index drives mean recruitment down by about 10% compared to the zero-trend model (Table 6.4, $\bar{R}_{2024-2053}$) reducing the stock's long-term average under any fishing level. At the end of the proection, 2053 recruitment was down by about 18.5% ((Table 6.4, R_{2053}). As a result, the 2053 spawning biomass was about 14% lower than the zero-trend model (Table 6.4, SSB_{2053}). Mean trends in biomass under the 20% lower model diverge slightly from the base model around 2038 but match the base model closely before that time (Figure 8.6).

Spring bloom timing models

Projections of the spring bloom timing model differ more from the base model than the copepod abundance model. Under constant spring bloom timing in the future, 3M cod spawning biomass, recruitment, and catch are a little higher than the base model, by similar amounts to the zero-trend copepod abundance model (Table 6.5, Figure 7.15). As above, the reduced process error variation and parameter uncertainty is the reason for slightly higher spawning biomass, recruitment, and catch under all fishing mortality rates.

Later spring bloom timing

Productivity is lower when spring bloom timing moves 20% later than the historical average over the next 30 years (i.e., a positive trend over the projection). The average recruitment in the projection period drops by about 10% (Table 6.5, $\bar{R}_{2024-2053}$), reaching 20% lower by the end of the projection (Table 6.5, $\bar{R}_{2024-2053}$). As a result, spawning biomass in 2053 is about 13% - 15% lower (Table 6.5, SSB_{2053}). When compared to the base model, the later spring bloom timing model has higher average recruitment for the earlier part of the time series. The early boost in recruitment increases spawning biomass for the 2028 - 2044 period, after which the mean spawning biomass series from the base model and spring bloom timing come closer together, differing by about 5% - 10% (Figure 8.7).

Earlier spring bloom timing

Productivity is higher when spring bloom timing is 20% earlier than the historical average after 30 years (i.e., a negative trend over the projection). As above, average recruitment increases by about 10% over the entire projection period and 18% in the final year (Table 6.5, $\bar{R}_{2024:2053}$, R_{2053}). Increasing recruitment drives spawning biomass from the spring bloom models to diverge from the base model after about 4 years, similar to above, and reach an equilibrium of about 15% higher under any fishing level (Table 6.5, SSB_{2053}, Figure 8.8).

3.2. Witch Flounder

3.2.1. Comparison of surplus production models

There were some notable differences to the original Witch Flounder stock assessment model when we fit the alternative TMB SSPM for Witch Flounder. While biomass estimates in the early and middle part of the time series are similar (Figure 7.12, upper panel), the carrying capacity K parameter is about 11% higher and intrinsic rate of growth r parameter about 34% lower (Table 6.6). The SSPM estimates are lower for the 1994 - 2014 period and do not show the large 'notch'-like decrease in biomass around 2013-2015 that occured in the original model (Figure 7.12). Instead, the SSPM estimates are more of a smooth wave during that period, with a slight dip before the stock resumes growing. Lower inter-annual variability in biomass is caused by process error estimates from the SSPM that have relatively low variance (the effective standard error is $\hat{\sigma} = 0.019$). SSPM estimates of process errors still have a similar pattern to the original model, except they are more informative and appear highly autocorrelated. Process errors take a 'walk' to about negative 3 standard deviations, with the largest deviation 2014 before gradually declining in magnitude until 2020 (Figure 7.12, lower panel).

3.2.2. Environmental covariates

Results of the correlation analysis indicated that zooplankton biomass had the highest correlation with annual Witch Flounder process errors (Figures 7.8 - 7.9, $\rho = +0.50$). Several of the NL climate indices (SST, S27.T, S27.CIL, Bottom.T, and Air.Temp) had moderate negative correlations with process errors with ρ ranging from -0.44 to -0.33.

Correlations among Witch Flounder process errors and 1 to 10 year lagged environmental indices are shown in Table 6.2, which we used to identify lagged indices with the strongest correlations to further consider as covariates in the SSPM. These included:

- 9-year lagged mean monthly SST ($\rho = -0.44$)
- 3-year lagged spring bloom timing ($\rho = 0.51$)
- 4-year lagged spring bloom intensity ($\rho = -0.45$)
- 1-year lagged zooplankton ($\rho = 0.43$)
- 8-year lagged composite climate index ($\rho = -0.45$)
- 8-year lagged sea ice ($\rho = 0.57$)
- 3-year lagged S27.T ($\rho = -0.50$)
- 8-year lagged CIL.area ($\rho = 0.45$),
- 8-year lagged NL climate index ($\rho = -0.50$).

Bottom temperature was also correlated with process errors at lags 1 to 8 but was not selected because it is strongly collinear with S27.T index. Although the zero lag zooplankton index was more correlated ($\rho = 0.43$), we considered a 1-year lag because there is a stronger biological rationale for an influence on Witch Flounder biomass, given that the production term in the Witch Flounder model integrates several years of recruitment, growth, and mortality.

We narrowed the set of indices further by fitting linear models with process errors as the response and indices as the explanatory variable, similar to the planned implementation in the stock assessment models (Figure 7.10). The most informative indices were the 8-year lagged sea ice index ($R^2 = 0.36$) and 4-year

lagged spring bloom intensity ($R^2 = 0.31$), which accounted for the most variation in the Witch Flounder process errors.

3.2.3. Model fits with and without environmental indices

Modeling the 3NO Witch Flounder population with environmental indices had a larger effect on recent biomass dynamics than on model parameters. For all three models, the carrying capacity K and intrinsic rate of growth r parameters are within 3% of the base model estimate (Table 6.7). As such, MSY-based model equilibria and the biomass time-series estimates in the early years of all three models are almost identical.

Differences in estimates of biomass among models started to appear once process error series began in 1984 (Figure 7.16). After covariates were included in process errors (1990 for the lagged Sea Ice model and 2006 for the lagged spring bloom timing model) there was visibly higher inter-annual variation in biomass estimates, with the largest differences after 2010 (Figure 7.16). In recent years, the spring bloom timing and base model agree on average trends in biomass, both recording a drop in biomass in 2015 from the large negative process error but then increasing towards the end of the historical period. In contrast, the sea ice model biomass has declined on average since 2011 and ends at 16.7 kt in 2023, versus around 30 kt in the base and spring bloom timing models. As a result of the lower biomass under the sea ice model, the 2023 harvest rate is about 77% higher than under the base and spring bloom timing models (Table 6.7).

Like the cod model above, environmental indices account for a large portion of the total variance in estimated process errors η_t. The portion of total variance in η_t accounted for by the covariate is 96% for the sea ice model and 86% for the spring bloom timing model (Table 6.7, $SD(\eta)$ vs $\hat{\sigma}$). The higher proportion of process error variance attributed to the covariates than initially observed in correlation analyses arises because the covariates inflate the estimated total process error variance in the SSPM (Table 6.7, $SD(\eta)$). Process error variance inflation arises because variation in the survey indices are high relative to the small increase in process error variance (Table 6.6, τ) (i.e., there is plenty of wiggle room within the total observation + process noise); in other words, there is substantial room for confounding between observation and process errors because of the simplified structure of state-space production models. In contrast, confounding is less prevalent in the age-structured model for cod because recruitment variability has a more direct connection to the observed age-composition data.

3.2.4. Projections with and without environmental indices

Sea ice model, lag 8

The sea ice index covariate for biomass process errors drives significant differences between the sea ice model and base model in projections. As outlined above, biomass estimates from the sea ice model are about 40% lower than the base model at the end of the historical period given low (lagged) sea ice index values at that time.

When projections assume that sea ice extent will vary around the historical average (zero-trend), production remains about the same as the base model given the similar r and K parameters. However, the sea ice model biomass remains lower than the base model biomass for most of the projection period, given its lower starting value and the 8-year lag bringing recent below average sea ice index values into the projection. The lag between the sea ice model and base model is consistent for the whole projection (Figure 7.17, top row). Final mean biomass B_{2053} under the sea ice model is 56% - 68% of the base model, with the smallest difference under the limit harvest rate U_{lim} (Table 6.8, Zero-Trend, Limit harvest rate).

Increasing sea ice extent

Witch Flounder production increases if sea ice extent increases by about 20% on average over the next 30 years. As a result, 2053 biomass ranges from around 34.5 kt at the limit harvest rate to around 76 kt with no fishing, which is around 10% - 11% above the zero-trend assumption. Despite the higher production, biomass under any fishing level is still unable to overcome the lower starting point in 2023, as well as the lower average production for the first 8 years of the projections, driven by the true sea ice index data (Table 6.8).

Decreasing sea ice extent

Witch Flounder production decreases and biomass grows more slowly when sea ice extent declines by 20% on average (Figure 8.12; Table 6.8, 20% lower). The mean biomass in 2052 is around 9% - 11% lower than the zero-trend model, and catch is about 3% - 4% lower, similar to the difference between the zero-trend and increase sea-ice model. Over time, biomass lags further behind the base model, and mean 2052 biomass is 39% - 50% lower than the base model (Table 6.8).

Spring bloom timing, lag 3

The 2023 biomass estimates from the lagged spring bloom timing model and the base model are almost identical so they have the same U_{squo} of 0.9% in projections. As above, the trends in spring bloom timing projections have the largest influence on final outcomes, and later spring bloom timing is associated with positive process errors, resulting in higher biomass.

If spring bloom timing varies around the historical average over the projection (i.e., zero-trend), production is similar to the base model. Indeed, the main difference between the base model and spring bloom timing model with zero projected trend is the uncertainty in future biomass, with the spring bloom timing model showing increased variation given the noisier index (Figure 7.18). Mean biomass values are very close. For example, the final year mean biomass B_{2053} for the spring bloom timing model is 3% - 5% higher than the base model across all harvest rates (Table 6.9). Yield is around 10% higher for the spring bloom timing model under the status quo harvest rate U_{2023}, and 11% higher for the limit harvest rate U_{lim} (Table 6.9).

Later bloom timing

Witch Flounder production increases when spring bloom timing moves later in the year during the projection (positive trend) and biomass grows faster than the base and zero-trend models (Figure 8.9; Table 6.9). Final year mean biomass B_{2053} is 8% - 11% higher than under the zero-trend case and yield is about 3% - 5% higher.

Earlier bloom timing

Finally, biomass grows more slowly than the base and zero-trend models if spring bloom timing moves earlier (Figure 8.10; Table 6.9). Results largely mirror the later bloom timing case. Terminal biomass B_{2053} is lower than the zero-trend model by the same 8% - 1% range. Yield is also lower by about 3% - 5%, but remains higher than under the base model.

4. Discussion

This study demonstrates an approach for assessing potential climate change impacts on future stock dynamics by including key environmental drivers of stock productivity in stock assessments and projections. Outcomes for model projections that include environmental indices as covariates for productivity depend on the model structure. Environmental indices had a larger effect on projections of future stock responses for an age structured model with compositional data informing productivity estimates compared to the simpler state-space surplus production model, where covariates had an effect on both the model history and projections.

4.1. Task 1: Identify environmental variables that best account for yearly variability in recruitment for 3M Atlantic Cod and production in 3NO Witch Flounder models.

The correlation analyses indicated copepod abundance and a 1-year lagged spring bloom timing accounted for the most variability in Atlantic Cod recruitment deviations. For the former, we found that higher copepod abundance on the Flemish Cap from 1999-2020 was associated with positive recruitment deviations. This may reflect improved foraging conditions and survival rates for larval and juvenile Atlantic Cod, for which copepods are key prey (Lough, Broughton, and Kristiansen 2017; Vikebø et al. 2021; Ruiz-Díaz, Dominguez-Petit, and Saborido-Rey 2022). An earlier spring bloom (a negative index in Figure 7.7) in the previous year

linked to higher recruitment is consistent with previous studies for Atlantic Cod indicating that an earlier spring bloom provides more overlap time for Cod larvae with abundant prey and increased growth and larval survival (Kristiansen et al. 2011; Jacobsen et al. 2022).

For Witch Flounder, we found that lagged indices for spring bloom timing (3-year lag) and NL sea ice cover (8-year lag) accounted for the most variation in biomass process errors. In contrast to Atlantic Cod, later spring bloom timing (a positive index in Figure 7.7) was associated with positive biomass deviations from the surplus production model. Given that Witch Flounder likely first appear in the survey around ages 3-5 (D. Swain et al. 2012), correlations with the lag-3 bloom timing index may be related to larval or juvenile survival. Witch Flounder has a longer pelagic stage and metamorphoses at larger sizes than most other flatfish in the Northwest Atlantic (Scott and Scott 1988; Rabe and Brown 2001), which may explain differences observed in spring bloom timing effects between Cod and Witch Flounder correlation analyses. Laboratory studies have indicated that Witch Flounder larvae growth and survival are unaffected by lower prey densities (Rabe and Brown 2001), in which case delayed spring bloom timing may lead to other ecosystem conditions that benefit larval or juvenile survival such as temperature, prey species composition, or predator densities (Rabe and Brown 2001).

With respect to sea ice, we found NL sea ice cover with an 8-year lag was positively correlated with Witch Flounder biomass process errors. Given the 8-year lag, this index is more likely to influence juvenile or sub adult survival, which may show up in survey indices 8 years later. Sea ice cover can influence shallow marine substrate environments via reduced sedimentation and light availability, which are key drivers for benthic communities (Kortsch et al. 2012; Clark et al. 2017). For example, sea ice might influence concentrations of bristle worms (polychaetes), crustaceans, or other benthic species (McConnell et al. 2012; Clark et al. 2017) that serve as key prey for Witch Flounder (Cargnelli 1999). The extent of sea ice cover rarely extends south of 45 degrees latitude into the 3NO Witch Flounder stock area, but it commonly covers the adjacent 2J3KL stock area in the north (DFO 2022). Therefore, it could be that sea ice cover influences survival of Witch Flounder in more northern habitats that move into 3NO at some stage. Alternatively, reduction of sea ice cover in 2J3KL may affect survival conditions more directly in 3NO through some other mechanism or it may be linked to other environmental conditions influencing survival not yet considered.

4.2. Tasks 2 and 3: Environmental Effects on Assessment Models and Projections

Task 2: *Demonstrate methods for incorporating selected environmental variables into current stock assessments for both species, to consider how estimates of life history parameters, stock status, and management related parameters (e.g., reference points) change when environmental covariates are included.*

Task 3: *Project original and modified stock assessment models incorporating environmental covariates to compare stock responses to fishing.*

Overall, including environmental covariates in assessment models had the largest effect on future projections for both stocks whereas estimates of model parameters and reference points were not significantly different from the base model with no covariates. While historical biomass estimates for 3M Cod were basically identical for models with and without environmental effects, biomass estimates toward the end of the history for 3NO Witch Flounder differed when including environmental effects. The largest difference was in the sea ice extent model, where biomass trends diverged significantly for the 2012 - 2023 period, but were more similar before that time. The divergence leads to a much higher 2023 'status quo' harvest rate of 1.6%, but it is still below the limit harvest rate of about 4%. In the spring bloom timing Witch Flounder model, biomass after 2012 has a similar average trend to the base model, but more inter-annual variability over the 2006 - 2020 period.

Projections for alternative environmental scenarios show that the impacts of environmental indices on productivity behave largely as expected. When environmental indices are positively correlated with process errors (e.g., sea ice for Witch Flounder, copepod abundance for Cod), then an increase in that variable will lead to higher stock productivity, and vice versa. If a climate variable has a negative relationship with process

errors (e.g., spring bloom timing for Cod), then productivity will increase when indices decrease, and vice versa.

Assessment model parameter and reference point estimates may be more influenced by model priors and assumptions than environmental indices in both stock assessment models. For example, the mean age-1 recruitment value for 3M Cod was fixed at 45 million age-1 fish (Garrido, González-Troncoso, and González-Costas 2024), which essentially anchors the size of the stock to that assumed value. Environmental covariates in this case act as deviations around that value. The highly variable recruitment process errors (a standard error of 2.05 under the base model) are then able to soak up the remaining recruitment variability and effectively reproduce the base model, leading to the same reference point estimates. Similarly, while priors on the carrying capacity K and intrinsic rate of growth r do not exert an overly strong influence on model estimates, the lack of sensitivity of those parameters may indicate that some priors are more influential than they appear.

For this analysis, we were limited in both cases to using environmental indices as covariates for process error by the structure of stock assessment models. For 3M Cod, the age-structured stock assessment model estimates age-1 recruitment and age-dependent mortality, but does not estimate time-varying natural mortality, precluding investigation of models considering climate impacts on survival. Moreover, growth, which may also be influenced by climate, is not modeled for 3M Cod but included via empirical weight-at-length observations from commercial catch and survey records. For 3NO Witch Flounder, the surplus production model structure also limits options for investigating climate impacts on stock dynamics, since multiple years of stock productivity are integrated into the single production term (i.e., biomass).

4.3. Task 4: Identify additional approaches or tools to support NAFO considering climate change impacts within Scientific Council and Commission's decision-making process.

The research recommendations below each include a qualitative estimate of the level of analyst time to implement the recommendation (e.g., low, medium, high) and perceived impact (e.g., medium, high) on management advice

1. **Simulation approach to evaluate management outcomes where assessment models incorporate environmental covariates (high effort, high impact)**

Several conditions must occur if fishery outcomes are to be improved by incorporating environmental effects into stock assessment and management advice (see Figure 19 below). First, there must be a consistent environmental effect on stock productivity that persists into the future (Ransom A. Myers 1998) and there must be reliable data for environmental covariates. For example, the Pacific Decadal Oscillation (PDO) has been consistently linked over multiple assessment with recruitment regimes of Pacific Halibut (Stewart and Hicks 2024). Second, given that an environmental effect and reliable environmental index data are available, there must be sufficient statistical power to detect the effect while controlling the risk of spurious relationships (see recommendation 3). Third, if an effect exists and can be reliably detected, it must have a reasonably strong influence on management outcomes. The potential for improved management performance will vary depending on uncertainty in assessment models and projections, environmental monitoring data and future trends, and the magnitude of environmental effects on stock productivity. The ultimate management outcome remains uncertain for cases involving both true and spurious environmental effects since including an environmental process into stock assessment is subject to standard statistical and management risks.

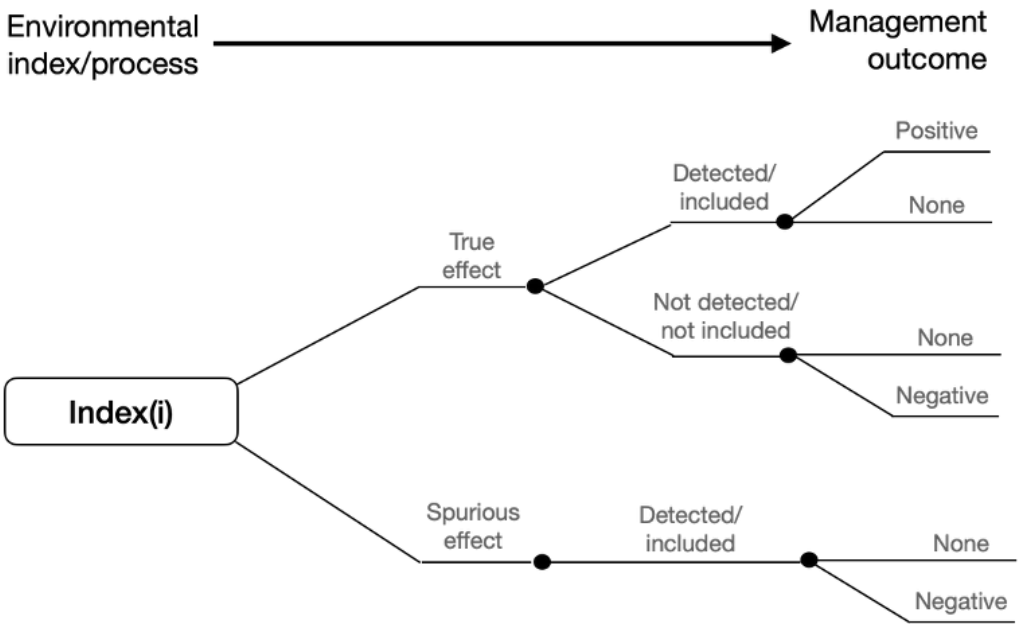

Figure 19. Potential paths involved when an index (i) is selected from a set of possible alternatives, whether that index has a true or spurious effect on the stock dynamics, whether that effect is detected and included in the assessment, and then whether the final management outcome is positive, neutral, or negative. Although this seems complicated, simulation models can be used to run through these pathways of effects over many candidate environmental indices since the above process is present for every index considered.

Closed loop simulation is increasingly used for rigorously testing fishery decision making frameworks in the presence of uncertainties, including those arising from uncertain environmental dynamics (André E. Punt et al. 2016; de la Mare 1998). There are two places where an MSE process could include environmental indices. First, stock assessment models fit to environmental covariates could be used to develop operating model scenarios, which would then be used to test the robustness of candidate decision making procedures to uncertainties about those indices. The results of such an exercise would provide insights about the expected management outcomes under a range of future climate scenarios (Wildermuth et al. 2023; André E. Punt et al. 2021). Second, environmental variables can be included in management procedures (MPs) either in the stock assessment or in harvest control rules (Wildermuth et al. 2023). A set of candidate MPs, including those with and without links to environmental indices, could then be tested against operating models that reflect a range of scenarios for environmental effects on stock productivity and future climate conditions.

The steps involved in closed-loop simulation are described in numerous papers (e.g., Cox, Kronlund, and Wyeth 2010). The main initial objective for NAFO stocks would be to provide valuable insights into potential benefits (and risks) of including environmental effects under different conditions, including a range of effect sizes, detectability, and proportion of variance accounted for by covariates. For example, an Environmental Effects Evaluation Checklist (EEEC) could be developed from the simulations that includes a 2x2 outcome matrix with probabilities for correctly detecting environmental effects (yes/no) and improved management outcomes (yes/no) under OM scenarios with varying correlations and effect sizes for environmental covariates. This could serve as a guide or initial step for informing future research efforts that have higher potential to improve management outcomes.

2. Identify approaches for reliably forecasting environmental covariates (low-high effort, high impact)

Without reliable forecasts for environmental covariates, management outcomes will be contingent on speculative environmental scenarios rather than empirically supported forecasts, reducing the likelihood for improved results. The methods to project the environmental indices in this study used arbitrary choices for future index trends (e.g., constant/increasing/decreasing). Such choices were needed to demonstrate the approach given that projections of environmental indices covering 2024-2053 were not available for the selected covariates. Additionally, the estimated auto-correlation factors were quite low for three out of four indices (0.01 - 0.67), so some projections behave more like independent variation around the historical average than random walks. Despite this, projections provided useful insights related to expected outcomes for stock biomass and catch under target harvest rates for future scenarios; however, they did not provide clear direction to management on which scenario to use for management advice. For example, if it is not well understood how spring bloom timing is expected to change in the future in response to climate change (Edwards and Richardson 2004; Neuheimer et al. 2010; Maillet et al. 2019; Friedland et al. 2024), then there will be challenges for how managers weight the three spring bloom timing scenarios in decision making (note that the above simulation approach and suggested EEEC could help with that). Similarly, while future sea ice extent is expected to decline, suggesting lower future Witch Flounder production, the magnitude and rate of decline remain uncertain. Our projections do not address this uncertainty given the arbitrary choice for future sea ice trends (i.e., 20% decline over 30 years).

Information for decision making could be improved if all environmental indices considered for assessment modeling had validated forecasting approaches (e.g., climate models). This might involve limiting the suite of indices considered in the model selection stage to those with existing predictive models (low effort) or developing new forecasting methods (high effort). For example, some indices may be strongly correlated with other environmental indices that have existing forecasting models. One such index might be copepod abundance, which can be modeled based on temperature and chlorophyll-a (Neuheimer et al. 2010), while existing climate models (CMIP6, Community Earth System Model) could be used for projecting sea ice cover (Fol et al. 2025; Chang et al. 2020). Projections based on modeled indices could also incorporate model uncertainty for those indices. Finally, linking stock productivity to lagged variables may improve short-term tactical decision making. The lagged variables used here provide 1 - 8 years of real data, which would provide an expectation of near-term productivity and reduce the uncertainty in short-term projections used for setting catch limits.

3. Large-scale meta-analysis to reduce the risk of spurious relationships (medium effort, medium impact)

As noted in the event tree above (Figure 19), detecting spurious environmental effects on productivity is a tangible risk in fisheries stock assessment. Future work should include a more robust evaluation of potential mechanisms by which environmental (e.g., spring bloom timing, copepod abundance, sea ice extent) and other covariates may affect stock dynamics prior to integrating these into assessment models and management advice. Identification of spurious relationships between fish stock dynamics and environmental indices is common, and perceived relationships from historical data often break down over time (Lapointe and Peterman 1991; Ransom A. Myers 1998). Above, we proposed some hypotheses to explain potential environmental effects on Cod recruitment and Witch Flounder biomass (4.1) but a more comprehensive analysis and literature review could be conducted.

There are other potential drivers of changing stock productivity not considered in this study that could be evaluated, such as increased predator population impacts on mortality rates. For example, increasing marine mammal populations have been linked to rising natural mortality rates for a variety of fish species, including Pacific Herring, Chinook Salmon, Atlantic Cod, and White Hake (Benoît et al. 2011; D. P. Swain and Benoit 2015; Chasco et al. 2017; Neuenhoff et al. 2019; Doherty et al. 2024; Rossi, Cox, and Benoît 2024). Many marine mammal populations have experienced rapid population growth since the 1960s following the end of commercial harvest and predator control programs (Magera 2013; Doherty et al. 2024), including Grey Seals

in NAFO stock areas (Neuenhoff et al. 2019; Rossi et al. 2021). Marine mammal population increases may be strongly correlated with temperature or other environmental indices with consistent increasing trends in recent years, complicating model selection. This highlights the importance of initial hypotheses development and careful selection of covariates considered, increasing the chances of identifying the key drivers of stock productivity while reducing opportunities for collinear variables (Doherty, Rossi, and Cox 2022; James et al. 2023).

A hierarchical approach to assessing environmental effects on stock productivity for multiple stocks (Malick et al. 2015, 2017; Doherty, Rossi, and Cox 2022) could also be explored, whereby increased statistical power associated with higher sample sizes can decrease uncertainty in estimated effects sizes and reduce spurious relationships (Ransom A. Myers and Mertz 1998; Mueter, Peterman, and Pyper 2002). For example, a hierarchical meta-analysis could potentially include multi-stock models for NAFO stocks for Atlantic Cod (2J3KL, 3Pn4RS, 3Ps, 3L, 3M, 3NO, 4T-Vn, 4X5Y) and Witch Flounder (2J3KL, 3Ps, 3NO, 4RST) depending on the availability of process errors from stock assessments. By sharing information across multiple stocks, hierarchical models may also extend time series of environmental indices and process errors available for analyses and consider spatial correlations (Su, Peterman, and Haeseker 2004; Mueter, Peterman, and Pyper 2002; Malick, Hunsicker, et al. 2020). This approach might also provide insights into shifts in species distribution that may be occurring due to climate change, whereby some stocks may appear to experience different trends in stock productivity that are influenced by migration from adjacent stock areas.

4. Investigate climate-driven shifts in species distribution for NAFO stocks (medium effort, medium impact)

Shifts in species distribution and suitable thermal habitats are probably the most predictable climate change impacts on NAFO stocks, whereby marine species may move north and into deeper waters relative to their historical ranges (Nye et al. 2009; Kleisner et al. 2017; Cote et al. 2021). For example, northward shifts in species distribution have been observed in the Northeastern US for Black Seabass (*Centropristis striata*), Scup (*tenotomus chrysops*), and Summer Flounder (*Paralichthys dentatus*) (Bell et al. 2015). Changing species distributions related to climate change are expected to be more prevalent in fishes than mammals and birds given the more direct thermal effects of warming water on fish physiology (Campana et al. 2020), creating challenges for stock assessment, fisheries management, commercial fisheries, seafood markets, and local economies (Oremus 2019; Baudron et al. 2020; Gullestad, Sundby, and Kjesbu 2020).

Climate-driven shifts in species distribution can be more directly observed than other climate effects on fish stocks (Campana et al. 2020), some of which may have varying effects according to life-history (Malick, Hunsicker, et al. 2020; Cote et al. 2021). Changes in fish density over space and time can be observed in fisheries and survey data, as long as commercial fishing or survey sampling occur in the new habitat areas (Nye et al. 2009; Bell et al. 2015). While NAFO stocks may be shifting their distribution in response to climate change, there remains considerable uncertainty about how these changes may impact fish population dynamics and stock-level productivity. A study of the Northeast US shelf found that over 50% of studied species show high to very high potential for a change in distribution with anticipated negative effects on the stock (including Witch Flounder and Atlantic Cod), although there was high uncertainty in potential distribution shifts for at least half the species assessed (Hare et al. 2016).

Changes in species distribution to adjust to rising temperatures can alter migration rates across adjacent stock boundaries, which may affect estimates of life history and productivity parameters in stock assessment. For example, if there is significant increase in the portion of fish emigrating north of stock area boundaries, then models may estimate higher natural mortality. Conversely, a large immigration of fish into a stock area that is more thermally suitable may be interpreted as increased recruitment or reduced natural mortality, particularly if the latter is age-dependent. Given that climate-driven migrations may occur over short time periods relative to a stock's historical assessment period, migration effects would first appear in annual process error terms for recruitment and mortality and would also eventually affect long-term average life history traits, such as carrying capacity. Interestingly, the potential for shifts in productivity also vary inversely with the potential for shifts in distribution across species (Hare et al. 2016). In other words, marine

species migration in response to rising temperatures may allow species to reduce overall productivity changes across their full habitat range; however, this may not be the case for individual management units using spatial boundaries that subdivide species habitats. For a stock management unit, higher potential for migration from one stock area to another likely corresponds to higher potential for changing stock productivity within the affected stock areas. Changes in spatial and temporal overlap of predators and prey can also lead to changes in mortality or improved recruitment via impacts to survival for different life-history stages. For example, a reduced overlap between marine mammals with key forage fish prey species could lead to reduced forage fish mortality rates (Sadykova et al. 2020). Growth rates and size-at-age could also be impacted by changing energetic availability from climate-related shifts in diets or density dependent effects from changing densities related to new habitat areas (Malick et al. 2017; Gauzens et al. 2024). By accounting for changes in species distribution and potential time-varying effects on stock productivity, analysts can improve information for stock assessment and projections used for management advice.

5. Changes to stock assessment models (medium effort, medium impact)

3M Cod - Future work should consider modifying assessment models to include stock-recruitment relationships. For instance, the 3M Atlantic Cod stock assessment model assumes that recruitment is independent of spawning biomass, which means there is probably some confounding of environmental effects with changes in spawning biomass. Estimated recruitment process errors currently have very large negative values during the recruitment failure that led to the collapse in the 1990s, when recruitments fell to record lows around 2-3 standard errors below the mean. A stock recruitment model produces lower recruitment, on average, at such low spawning biomass and recruitment process errors would have a smaller magnitude in post-collapse years. The resulting process error estimates may show correlations to a different set of climate indices that those included here.

3NO With Flounder - The current 3NO Witch flounder surplus production model needs a prior predictive check to understand the influence of priors on its parameters and results. A prior-predictive check runs the assessment using parameters sampled from the priors only. This would indicate the extent to which the assessment results depend on priors vs the data.

In addition to the insensitivity of life history parameters mentioned above, we could not estimate the initial biomass relative to carrying capacity (or depletion) parameter in the substitute TMB surplus production model. As discussed elsewhere, there were no survey biomass indices before 1984 to provide a basis, so no data was available for the estimation of initial depletion. Our The TMB model first estimates maximum posterior density estimates via optimisation of the objective function, and the estimates of parameter standard errors using the δ-method are part of our check for convergence. For initial depletion, indicated that standard errors were not finite for the initial biomass, which is a classic symptom of an uninformed parameter.

The TMB state-space surplus production model may require reparameterisation if it is to be used as the new 3NO Witch Flounder stock assessment model in the future. Under the current parameterisation, we could not sample an acceptable Bayes posterior because there were a small number of divergent transitions during Hamiltonian Monte Carlo sampling. Divergent transitions are usually associated with parts of the objective function that have very high gradients indicating that a portion of the posterior was unable to be sampled, and therefore model estimates and their uncertainty are probably biased. Divergent transitions are relatively common for state-space production models in the absence of penalty functions (Best and Punt 2020).

There is potential for bias in estimates of 3NO Witch Flounder stock productivity and carrying capacity caused by uncertain catch data. Prior to 1973, Witch Flounder catches are reconstructed from early aggregated flatfish catches and are suggested to be viewed with caution, while survey biomass indices only start in 1984 (Maddock Parsons, Skanes, and Rideout 2024). As such, early biomass levels are based solely on several years of reconstructed catch, likely inducing bias in the carrying capacity K. This could in turn bias the intrinsic rate of growth r, given that r and K are negatively correlated. We recommend sensitivity analyses for r and K under alternative catch reconstruction scenarios to better understand potential bias.

Provided that estimated environmental relationships to productivity are not spurious, environmental indices could inform process errors in years with missing data. For 3NO Witch Flounder, lack of survey indices prior to 1984 means that there is no information to estimate Witch Flounder process errors for the earlier period. As a result, models are treated as deterministic from 1960 to 1983, potentially biasing estimates of other parameters. An environmental index that includes years before 1984 could be used to partially fill that gap by back-casting the process error component, potentially reducing bias in parameters by modeling the variation in production before 1984.

4.4. Conclusion

Environmental covariates in 3M Cod and 3NO Witch Flounder stock assessments accounted for 20% to 96% of the estimated variation in stock productivity, although the latter variance was inflated because of possible confounding with observation uncertainty. Incorporating these environmental indices into stock assessments and 30-year projections suggests potential long-term climate impacts on stock productivity, biomass, and catch. We provide five recommendations that should be considered next before incorporating environmental covariates into management advice. First, use closed-loop simulations to evaluate the extent to which incorporating environmental factors in stock assessment could improve management outcomes under climate change. Second, develop reliable projection models for environmental variables that are linked to productivity and would have a reasonable chance of improving management outcomes. Third, use meta-analysis informed by plausible biological mechanisms to reduce the risk of spurious relationships between environmental covariates and productivity. Fourth, investigate climate-driven shifts in species distribution that may influence migration rates between stock boundaries and estimates of stock-level productivity. Finally, update stock assessment models to provide more information for evaluating links between environmental indices and indicators of stock productivity. These recommendations offer a practical roadmap to guide future research planning and to establish well-documented methods to assess climate change impacts in NAFO stock assessment and management advice.

5. References

Baudron, A. R., Brunel, T., Blanchet, M.-A., Hidalgo, M., Chust, G., Brown, E. J., Kleisner, K. M., Millar, C., MacKenzie, B. R., Nikolioudakis, N., et al. (2020). Changing fish distributions challenge the effective management of European fisheries. *Ecography*, *43*(4), 494–505.

Bell, R. J., Richardson, D. E., Hare, J. A., Lynch, P. D., & Fratantoni, P. S. (2015). Disentangling the effects of climate, abundance, and size on the distribution of marine fish: An example based on four stocks from the Northeast US shelf. *ICES Journal of Marine Science*, *72*(5), 1311–1322.

Benoît, H. P., Swain, D. P., Bowen, W. D., Breed, G. A., Hammill, M. O., & Harvey, V. (2011). Evaluating the potential for grey seal predation to explain elevated natural mortality in three fish species in the southern gulf of st. lawrence. *Marine Ecology Progress Series*, *442*, 149–167.

Best, J. K., & Punt, A. E. (2020). Parameterizations for Bayesian state-space surplus production models. *Fisheries research*, *222*, 105411.

Campana, S. E., Stefánsdóttir, R. B., Jakobsdóttir, K., & Sólmundsson, J. (2020). Shifting fish distributions in warming sub-arctic oceans. *Scientific Reports*, *10*(1), 16448.

Cargnelli, L. M. (1999). Essential fish habitat source document. Witch flounder, *Glyptocephalus cynoglossus*, life history and habitat characteristics.

Chang, P., Zhang, S., Danabasoglu, G., Yeager, S. G., Fu, H., Wang, H., Castruccio, F. S., Chen, Y., Edwards, J., Fu, D Jia, Y., Laurindo, L. C., Liu, X., Rosenbloom, N.,Small, R. J., Xu, G., Zeng, Y., Zhang, Q., Bacmeister, J., … Wu, L. (2020). An unprecedented set of high-resolution earth system simulations for understanding multiscale interactions in climate variability and change. *Journal of Advances in Modeling Earth Systems*, *12*(12), e2020MS002298. https://doi.org/https://doi.org/10.1029/2020MS002298

Chasco, B. E., Kaplan, I. C., Thomas, A. C., Acevedo-Gutiérrez, A., Noren, D. P., Ford, M. J., Hanson, M. B., Scordino, J. J., Jeffries, S. J., Marshall, K. N., et al. (2017). Competing tradeoffs between increasing marine mammal predation and fisheries harvest of chinook salmon. *Scientific reports*, *7* (1), 15439.

Clark, G. F., Stark, J. S., Palmer, A. S., Riddle, M. J., & Johnston, E. L. (2017). The roles of sea-ice, light and sedimentation in structuring shallow Antarctic benthic communities. *PLoS One*, *12*(1), e0168391.

Cote, D., Konecny, C. A., Seiden, J., Hauser, T., Kristiansen, T., & Laurel, B. J. (2021). Forecasted shifts in thermal habitat for cod species in the Northwest Atlantic and Eastern Canadian Arctic. *Frontiers in Marine Science*, *8*, 764072.

Cox, S., Kronlund, A., & Wyeth, M. (2010). Development of precautionary management strategies for the British Columbia sablefish (*Anoplopoma fimbria)* fishery. *DFO Can. Sci. Advis. Sec. Res. Doc. 2009/043. vii + 145 p.*

Cyr, F., & Bélanger, D. (2024). Environmental indices for NAFO subareas 0 to 4 in support of the Standing Committee on Fisheries Science (STACFIS) – 2023 update. *NAFO SCR Doc. 24/012. Ser. No. N7515*.

Cyr, F., & Galbraith, P. S. (2020a). A climate index for the Newfoundland and Labrador shelf. *Earth System Science Data Discussions*, *2020*, 1–23.

Cyr, F., & Galbraith, P. S. (2020b). Newfoundland and Labrador climate index. *Federated Research Data Repository*, *Version 2023*. https://doi.org/10.20383/101.0301.

de la Mare, W. K. (1998). Tidier fisheries management requires a new MOP (management oriented paradigm). *Reviews in Fish Biology and Fisheries*, *8*(3), 349–356. https ://doi.org/10.1023/A:1008819416162

DFO. (2022). *Ice navigation in Canadian waters* (S. edition, Ed.). Fisheries; Oceans Canada.

Doherty, B., Johnson, S. D. N., Benson, A. J., Cox, S. P., Cleary, J. S., & Lane, J. (2024). Predation by marine mammals explains recent trends in natural mortality of pacific herring (*clupea pallasii*) and changes expectations for future biomass. *ICES Journal of Marine Science*, fsae183 https://doi.org/10.1093/icesjms/fsae183

Doherty, B., Rossi, S., & Cox, S. (2022). *Hatchery, predation, and climate effects on productivity of wild Chinook Coho, and Chum salmon* (tech. rep.). Pacific Salmon Foundation.

Edwards, M., & Richardson, A. J. (2004). Impact of climate change on marine pelagic phenology and trophic mismatch. *Nature*, *430*(7002), 881–884.

Fol, M., Tremblay, B., Pfirman, S., Newton, R., Howell, S., & Lemieux, J.-F. (2025). Revisiting the Last Ice Area projections from a high-resolution Global Earth System Model. *Communications Earth & Environment*, *6*(1), 46.

Friedland, K. D., Nielsen, J. M., Record, N. R., Brady, D. C., & Morrow, C. J. (2024). The phenology of the spring phytoplankton bloom in the North Atlantic does not trend with temperature. *Elementa: Science of the Anthropocene*, *12*(1).

Garrido, I., González-Troncoso, D., & González-Costas, F. (2024). *Assessment of the Cod Stock in NAFO Division 3M* (tech. rep. No. NAFO SCR Doc. 24/016, Serial No. N7521).

Gauzens, B., Rosenbaum, B., Kalinkat, G., Boy, T., Jochum, M., Kortsch, S., O'Gorman, E. J., & Brose, U. (2024). Flexible foraging behaviour increases predator vulnerability to climate change. *Nature climate change*, *14*(4), 387–392. GEBCO Compilation Group. (2024). *GEBCO 2024 Grid*.

Gullestad, P., Sundby, S., & Kjesbu, O. S. (2020). Management of transboundary and straddling fish stocks in the Northeast Atlantic in view of climate-induced shifts in spatial distribution. *Fish and Fisheries*, *21*(5), 1008–1026.

Haltuch, M., Brooks, E., Brodziak, J., Devine, J., Johnson, K., Klibansky, N., Nash, R., Payne, M., Shertzer, K., Subbey, S., et al. (2019). Unraveling the recruitment problem: A review of environmentally-informed forecasting and management strategy evaluation. *Fisheries Research*, *217*, 198–216.

Haltuch, M. A., Tolimieri, N., Lee, Q., & Jacox, M. G. (2020). Oceanographic drivers of petrale sole recruitment in the California Current Ecosystem. *Fisheries Oceanography*, *29*(2), 122–136.

Hare, J. A., Morrison, W. E., Nelson, M. W., Stachura, M. M., Teeters, E. J., Griffis, R. B., Alexander, M. A., Scott, J. D., Alade, L., Bell, R. J., et al. (2016). A vulnerability assessment of fish and invertebrates to climate change on the Northeast US Continental Shelf. *PloS one*, *11*(2), e0146756.

Holsman, K. K., Ianelli, J., Aydin, K., Punt, A. E., & Moffitt, E. A. (2016). A comparison of fisheries biological reference points estimated from temperature-specific multi-species and single-species climate-enhanced stock assessment models. *Deep Sea Research Part II: Topical Studies in Oceanography*, *134*, 360–378. https://doi.org/0.1016/j.dsr2.2015.08.001

Jacobsen, S., Nielsen, K. K., Kristiansen, R., Grønkjær, P., Gaard, E., & Steingrund, P. (2022). Influence of larval prey availability on year class strength in Faroe Plateau cod *(Gadus morhua)*. *Marine Biology*, *169*(12), 153.

James, S. E., Doherty, B., Cox, S. P., Pearsall, I. A., & Riddell, B. (2023). Size and timing of hatchery releases influence juvenile-to-adult survival rates of british columbia chinook (oncorhynchus tshawytscha) and coho (oncorhynchus kisutch) salmon. *Canadian Journal of Fisheries and Aquatic Sciences*, *00*(1-19). https://doi.org/10.1139/cjfas- 2022-0121

Karp, M. A., Peterson, J. O., Lynch, P. D., Griffis, R. B., Adams, C. F., Arnold, W. S., Barnett, L. A., deReynier, Y., DiCosimo, J., Fenske, K. H., et al. (2019). Accounting for shifting distributions and changing productivity in the development of scientific advice for fishery management. *ICES Journal of Marine Science*, *76*(5), 1305–1315.

Khalsa, N. S., Hodgdon, C. T., Mazur, M. D., & Chen, Y. (2023). Climate-driven shifts in growth and maturity induce changes to the population and fishery dynamics of a high-value crustacean. *Fisheries Research*, *259*, 106574.

Kleisner, K. M., Fogarty, M. J., McGee, S., Hare, J. A., Moret, S., Perretti, C. T., & Saba, V. S. (2017). Marine species distribution shifts on the us northeast continental shelf under continued ocean warming. *Progress in Oceanography*, *153*, 24–36.

Kortsch, S., Primicerio, R., Beuchel, F., Renaud, P. E., Rodrigues, J., Lønne, O. J., & Gulliksen, B. (2012). Climate-driven regime shifts in Arctic marine benthos. *Proceedings of the National Academy of Sciences*, *109*(35), 14052–14057.

Kristensen, K., Nielsen, A., Berg, C. W., Skaug, H., & Bell, B. M. (2016). TMB: Automatic differentiation and Laplace approximation. *Journal of Statistical Software*, *70*(5), 1– 21. https://doi.org/10.18637/jss.v070.i05

Kristiansen, T., Drinkwater, K. F., Lough, R. G., & Sundby, S. (2011). Recruitment variability in North Atlantic cod and match-mismatch dynamics. *PLoS one*, *6*(3), e17456.

Lapointe, M. F., & Peterman, R. M. (1991). Spurious correlations between fish recruitment and environmental factors due to errors in the natural mortality rate used in virtual population analysis (VPA). *ICES Journal of Marine Science*, *48*(2), 219–228.

Lough, R. G., Broughton, E. A., & Kristiansen, T. (2017). Changes in spatial and temporal variability of prey affect functional connectivity of larval and juvenile cod. *ICES Journal of Marine Science*, *74*(6), 1826–1837.

Maddock Parsons, D., Skanes, K., & Rideout, R. (2024). *An assessment of the Witch flounder resource in NAFO Divisions 3NO* (tech. rep. No. NAFO SCR Doc. 24/018, Serial No. N7523).

Magera, A. M., Mills Flemming, J. E., Kaschner, K., Christensen, L. B., & Lotze, H. K. (2013). Recovery trends in marine mammal populations. *PLOS ONE*, *8*(10), 1–12. https://doi.org/10.1371/journal.pone.0077908

Maillet, G., Bélanger, D., Doyle, G., Robar, A., Rastin, S., Ramsay, D., & Pepin, P. (2019). Optical, chemical, and biological oceanographic conditions on the Newfoundland and Labrador shelf during 2018. *Canadian Science Advisory Secretariat*, *2022/075*.

Malick, M. J., Cox, S. P., Mueter, F. J., Dorner, B., & Peterman, R. M. (2017). Effects of the North Pacific Current on the productivity of 163 Pacific salmon stocks. *Fisheries Oceanography*, *26*(3), 268–281.

Malick, M. J., Cox, S. P., Mueter, F. J., Peterman, R. M., & Bradford, M. (2015). Linking phytoplankton phenology to salmon productivity along a North–South gradient in the Northeast Pacific Ocean. *Canadian Journal of Fisheries and Aquatic Sciences*, *72*(5), 697–708.

Malick, M. J., Hunsicker, M. E., Haltuch, M. A., Parker-Stetter, S. L., Berger, A. M., & Marshall, K. N. (2020). Relationships between temperature and Pacific hake distribution vary across latitude and life-history stage. *Marine Ecology Progress Series*, *639*, 185–197.

Malick, M. J., Siedlecki, S. A., Norton, E. L., Kaplan, I. C., Haltuch, M. A., Hunsicker, M. E., Parker-Stetter, S. L., Marshall, K. N., Berger, A. M., Hermann, A. J., et al. (2020). Environmentally driven seasonal forecasts of Pacific hake distribution. *Frontiers in Marine Science*.

McConnell, B., Gradinger, R., Iken, K., & Bluhm, B. A. (2012). Growth rates of arctic juvenile Scolelepis squamata *(Polychaeta: Spionidae)* isolated from Chukchi Sea fast ice. *Polar biology*, *35*, 1487–1494.

Monnahan, C. C. (2024). Toward good practices for Bayesian data-rich fisheries stock assessments using a modern statistical workflow. *Fisheries Research*, *275*, 107024.

Monnahan, C. C., & Kristensen, K. (2018). No-u-turn sampling for fast Bayesian inference in ADMB and TMB: Introducing the adnuts and tmbstan R packages. *PloS one*, *13*(5), e0197954.

Mueter, F. J., Peterman, R. M., & Pyper, B. J. (2002). Opposite effects of ocean temperature on survival rates of 120 stocks of Pacific salmon *(Oncorhynchus spp.)* in northern and southern areas. *Canadian Journal of Fisheries and Aquatic Sciences*, *59*(3), 456–463.

Myers, R. A. (1998). When do environment–recruitment correlations work? *Reviews in Fish Biology and Fisheries*, *8*(3), 285–305. https://doi.org/10.1023/A:1008828730759

Myers, R. A., & Mertz, G. (1998). Reducing uncertainty in the biological basis of fisheries management by meta-analysis of data from many populations: A synthesis. *Fisheries Research*, *37* (1-3), 51–60.

Neuenhoff, R. D., Swain, D. P., Cox, S. P., McAllister, M. K., Trites, A. W., Walters, C. J., & Hammill, M. O. (2019). Continued decline of a collapsed population of atlantic cod (*Gadus morhua*) due to predation-driven allee effects. *Canadian Journal of Fisheries and Aquatic Sciences*, *76*(1), 168–184.

Neuheimer, A., Gentleman, W., Pepin, P., & Head, E. (2010). Explaining regional variability in copepod recruitment: Implications for a changing climate. *Progress in Oceanography*, *87* (1-4), 94–105.

Nye, J. A., Link, J. S., Hare, J. A., & Overholtz, W. J. (2009). Changing spatial distribution of fish stocks in relation to climate and population size on the Northeast United States continental shelf. *Marine Ecology Progress Series*, *393*, 111–129.

Oremus, K. L. (2019). Climate variability reduces employment in New England fisheries. *Proceedings of the National Academy of Sciences*, *116*(52), 26444–26449.

Punt, A. E. (2003). Extending production models to include process error in the population dynamics. *Canadian Journal of Fisheries and Aquatic Sciences*, *60*(10), 1217–1228. https://doi.org/10.1139/f03-105

Punt, A. E., Butterworth, D. S., Moor, C. L., De Oliveira, J. A. A., & Haddon, M. (2016). Management strategy evaluation: Best practices. *Fish and Fisheries*. https://doi.org/10.1111/faf.12104

Punt, A. E., Dalton, M. G., Cheng, W., Hermann, A. J., Holsman, K. K., Hurst, T. P., Ianelli, J. N., Kearney, K. A., McGilliard, C. R., Pilcher, D. J., et al. (2021). Evaluating the impact of climate and demographic variation on future prospects for fish stocks: An application for northern rock sole in Alaska. *Deep Sea Research Part II: Topical Studies in Oceanography*, *189*, 104951.

Punt, A. E., Dalton, M. G., & Foy, R. J. (2020). Multispecies yield and profit when exploitation rates vary spatially including the impact on mortality of ocean acidification on North Pacific crab stocks. *Fisheries Research*, *225*, 105481. https://doi.org/10.1016/j.fishres.2019.105481

Rabe, J., & Brown, J. A. (2001). The behavior, growth, and survival of Witch flounder *(Glyptocephalus cynoglossus)* larvae in relation to prey availability: Adaptations to an extended larval period. *Fishery Bulletin*, *99*(3), 465–465.

Rossi, S. P., Cox, S. P., & Benoît, H. P. (2024). Absence of predator control increases cod extirpation risk in a northwest atlantic ecosystem: Inference from multispecies modelling. *Marine Ecology Progress Series*, *746*, 99–119.

Rossi, S. P., Cox, S. P., Hammill, M. O., den Heyer, C. E., Swain, D. P., Mosnier, A., & Benoît, H. P. (2021). Forecasting the response of a recovered pinniped population to sustainable harvest strategies that reduce their impact as predators. *ICES Journal of Marine Science*, *78*(5), 1804–1814. https://doi.org/10.1093/icesjms/fsab088

Ruiz-Díaz, R., Dominguez-Petit, R., & Saborido-Rey, F. (2022). Atlantic cod growth history in Flemish Cap between 1981 and 2016: The impact of fishing and climate on growth performance. *Frontiers in Marine Science*, *9*, 876488.

Sadykova, D., Scott, B. E., De Dominicis, M., Wakelin, S. L., Wolf, J., & Sadykov, A. (2020). Ecological costs of climate change on marine predator–prey population distributions by 2050. *Ecology and Evolution*, *10*(2), 1069–1086.

Schaefer, M. B. (1957). Some considerations of population dynamics and economics in relation to the management of the commercial marine fisheries. *Journal of the Fisheries Board of Canada*, *14*(5), 669–681. https://doi.org/10.1139/f57-025

Scott, B. S., & Scott, M. G. (1988). *Atlantic fishes of Canada*. Can. Bull. Fish. Aquat. Sci. Spencer, P. D., Holsman, K. K., Zador, S., Bond, N. A., Mueter, F. J., Hollowed, A. B., & Ianelli, J. N. (2016). Modelling spatially dependent predation mortality of eastern Bering Sea walleye pollock, and its implications for stock dynamics under future climate scenarios. *ICES Journal of Marine Science*, *73*(5), 1330–1342.

Stewart, I., & Hicks, A. (2024). Assessment of the Pacific halibut *(Hippoglossus stenolepis)* stock at the end of 2024. *International Pacific Halibut Commission, Meeting Document IPHC-2025-SA-01, Seattle*.

Su, Z., Peterman, R. M., & Haeseker, S. L. (2004). Spatial hierarchical Bayesian models for stock-recruitment analysis of pink salmon *(Oncorhynchus gorbuscha)*. *Canadian Journal of Fisheries and Aquatic Sciences*, *61*(12), 2471–2486.

Swain, D. P., & Benoit, H. P. (2015). Extreme increases in natural mortality prevent recovery of collapsed fish populations in a northwest atlantic ecosystem. *Marine Ecology Progress Series*, *519*, 165–182.

Swain, D., Savoie, L., Aubry, É., & du Golfe, R. (2012). Assessment of Witch flounder *(Glyptocephalus cynoglossus)* in the Gulf of St. Lawrence (NAFO Divisions 4RST), February 2012. *Canadian Science Advisory Secretariat*, *2012/122*.

Tolimieri, N., Haltuch, M., Lee, Q., Jacox, M., & Bograd, S. J. (2018). Oceanographic drivers of sablefish recruitment in the California Current. *Fisheries Oceanography*, *27* (5), 458–474.

Vikebø, F. B., Broch, O. J., Endo, C. A. K., Frøysa, H. G., Carroll, J., Juselius, J., & Langangen, Ø. (2021). Northeast Arctic cod and prey match-mismatch in a highlatitude spring-bloom system. *Frontiers in Marine Science*, *8*, 767191.

Wang, Z., Brickman, D., Greenan, B., Christian, J., DeTracey, B., & Gilbert, D. (2023). Assessment of ocean temperature trends for the Scotian Shelf and Gulf of Maine using 22 CMIP6 Earth system models. *Atmosphere-Ocean*, *62*(1), 24–34.

Wildermuth, R. P., Tommasi, D., Kuriyama, P., Smith, J., & Kaplan, I. (2023). Evaluating robustness of harvest control rules to climate-driven variability in Pacific sardine recruitment. *Canadian Journal of Fisheries and Aquatic Sciences*, *81*(8), 1029–1051.

6. Tables

Table 1. Correlations between Atlantic Cod recruitment deviations and environmental indices from CMIP6 SST (Wang et al. 2024), STACFIS (Cyr & Bélanger, 2024), and Newfoundland and Labrador (Cyr & Galbraith, 2020a, 2020b) at 0-, 1-, and 2-year lags. The strongest correlations are shown in red.

Index	Lag 0	Lag 1	Lag 2
CMIP6 SST indices			
sst3M_high	0.16	0.27	0.4
sst3M_low	0.01	0.17	0.29
sst3M_mean	0.12	0.23	0.37
STACFIS environmental indices			
spring_bloom_timing3M	-0.24	-0.65	0
spring_bloom_intensity3M	0.11	0.21	0.22
copepod_abundance3M	0.48	0.42	0.46
zooplankton_biomass3M	0.33	0.31	0.11
composite_climate3M	-0.07	0.01	0.03
NL climate indices			
Wint.NAO	0.06	-0.02	-0.06
Air.Temp	-0.05	0.03	0.15
Sea.Ice	0.06	-0.08	-0.14
Icebergs	0.01	-0.19	-0.31
SST	-0.05	-0.06	0.04
S27.T	-0.05	0.13	0.19
S27.S	0.01	0.08	0.18
S27.CIL	-0.04	0.16	0.17
CIL.area	0.12	0	-0.05
Bottom.T	-0.01	0.12	0.12
Climate.index	-0.04	0.08	0.14

Table 2. Correlations between Witch Flounder process errors and environmental indices from CMIP6 SST (Wang et al. 2024), STACFIS (Cyr & Bélanger, 2024), and Newfoundland and Labrador (Cyr & Galbraith, 2020a, 2020b) 0- to 10-year lags. The strongest correlations are shown in red.

Index	0	-1	-2	-3	-4	-5	-6	-7	-8	-9	-10
CMIP6 SST indices											
sst3NO_high	-0.19	-0.24	-0.31	-0.27	-0.25	-0.32	-0.28	-0.33	-0.23	-0.19	-0.1
sst3NO_low	-0.1	-0.18	-0.16	-0.11	-0.06	-0.02	-0.1	-0.22	-0.32	-0.36	-0.31
sst3NO_mean	-0.17	-0.23	-0.23	-0.14	-0.1	-0.09	-0.16	-0.33	-0.39	-0.4	-0.34
STACFIS environmental indices											
spring_bloom_timing3LNO	0.24	0.34	0.38	0.52	0.48	0.36	0.01	-0.11	-0.1	-0.15	-0.28
spring_bloom_intensity3LNO	-0.04	-0.2	-0.26	-0.44	-0.43	-0.3	-0.15	0	0.2	0.38	0.31
copepod_abundance3LNO	-0.57	-0.5	-0.43	-0.32	-0.2	-0.05	0.06	0.14	0.24	0.34	0.4
zooplankton_biomass3LNO	0.43	0.37	0.22	0.11	0.01	0.03	-0.08	-0.2	-0.23	-0.2	-0.25
composite_climate3LNO	-0.3	-0.4	-0.44	-0.42	-0.39	-0.4	-0.46	-0.51	-0.52	-0.46	-0.41
NL climate indices											
Wint.NAO	-0.03	0.03	0.12	0.33	0.33	0.26	0.17	0.22	0.27	0.23	0.15
Air.Temp	-0.36	-0.4	-0.42	-0.49	-0.51	-0.56	-0.54	-0.57	-0.58	-0.57	-0.47
Sea.Ice	0.34	0.4	0.5	0.52	0.48	0.47	0.49	0.58	0.62	0.55	0.47
Icebergs	0.15	0.17	0.26	0.3	0.28	0.29	0.3	0.43	0.44	0.38	0.24
SST	-0.39	-0.45	-0.4	-0.32	-0.28	-0.36	-0.46	-0.48	-0.48	-0.46	-0.42
S27.T	-0.46	-0.49	-0.54	-0.56	-0.51	-0.46	-0.44	-0.49	-0.52	-0.5	-0.42
S27.S	0.26	0.23	0.23	0.28	0.26	0.17	0.01	-0.04	0.04	0.1	0.18
S27.CIL	-0.39	-0.37	-0.4	-0.45	-0.43	-0.36	-0.34	-0.38	-0.4	-0.37	-0.29
CIL.area	0.16	0.23	0.34	0.34	0.29	0.3	0.34	0.46	0.49	0.45	0.38
Bottom.T	-0.47	-0.52	-0.55	-0.54	-0.53	-0.52	-0.53	-0.53	-0.51	-0.45	-0.38
Climate.index	-0.38	-0.43	-0.49	-0.53	-0.5	-0.48	-0.48	-0.54	-0.57	-0.53	-0.44

Table 3. Estimated posterior mean values with standard errors for the 3M Atlantic Cod age-structured models under the base model without environmental covariates (Base) and the models fit the Copepod Abundance and Spring Bloom Timing (SB Timing) covariates. Estimated parameters shown include average recruitment $\bar{R}$, limit fishing mortality F_{lim}, environmental index coefficients α, recent average fishing mortality F_{sq}, residual recruitment process standard error $\hat{\sigma}$, 2023 spawning stock biomass SSB_{2023}, and 2023 recruitment R_{2023}.

	Base	Copepod Abundance	SB Timing
$\bar{R}$	45	45	45
F_{lim}	0.15 (0.011)	0.15 (0.012)	0.15 (0.011)
α_{Cope}		0.94 (0.418)	
α_{SpBl}			-0.91 (0.481)
F_{squo}	0.042 (0.004)	0.042 (0.004)	0.041 (0.004)
$\hat{\sigma}$	2.05 (0.018)	1.78 (0.068)	1.14 (0.127)
SSB_{2023}	27.46 (2.085)	27.42 (2.068)	27.55 (2.136)
R_{2023}	6.96 (2.086)	6.73 (2.028)	6.67 (2.071)

Table 4. Projected mean values with standard deviations for 3M Cod model with copepod covariate (Copepod AM) and without covariate (Base) over simulations under no fishing (F_0), recent average fishing mortality ($F_{squo} = \bar{F}_{2021-2023}$), and at the limit fishing mortality rate (F_{lim}). Copepod abdunance indices are projected under three scenarios assuming no future trend in the copepod abundance (zero trend), a positive trend (20% increase), and a negative trend (20% increase). Quantities shown are spawning biomass (SSB_{2053}) and recruitment (R_{2053}) at the end of the 30-year projection period, as well as mean recruitment ($\bar{R}_{2024-2053}$) and catch ($\bar{C}_{2024-2053}$) over projections. Biomass and catch units are in thousands of tonnes (kt), while recruitment is in millions (M) of fish.

Assessment Model + Index Scenario	SSB_{2053} (kt)	R_{2053} (M)	$\bar{R}_{2024-2053}$ (M)	$\bar{C}_{2024-2053}$ (kt)
F = 0, no fishing mortality				
Base	33.2 (51)	41.1 (185)	40.4 (32)	0.0 (0)
Copepod AM + zero trend	36.0 (62)	38.4 (128)	41.1 (28)	0.0 (0)
Copepod AM + 20% increase	41.1 (73)	46.3 (159)	45.3 (32)	0.0 (0)
Copepod AM + 20% decline	31.5 (54)	31.9 (104)	37.3 (25)	0.0 (0)
Recent average (status quo) fishing mortality rate				
Base	21.3 (36)	41.1 (185)	40.4 (32)	3.6 (2)
Copepod AM + zero trend	23.0 (43)	38.4 (128)	41.1 (28)	3.6 (2)
Copepod AM + 20% increase	26.3 (50)	46.3 (159)	45.3 (32)	3.8 (2)
Copepod AM + 20% decline	20.0 (37)	31.9 (104)	37.3 (25)	3.4 (2)
Limit fishing mortality rate				
Base	10.0 (19)	41.1 (185)	40.4 (32)	6.1 (3)
Copepod AM + zero trend	10.7 (21)	38.4 (128)	41.1 (28)	6.2 (3)
Copepod AM + 20% increase	12.3 (25)	46.3 (159)	45.3 (32)	6.5 (4)
Copepod AM + 20% decline	9.3 (18)	31.9 (104)	37.3 (25)	5.9 (3)

Table 5. Projected mean values with standard deviations for 3M Cod model with spring bloom timing covariate (SB Timing AM) and without covariate (Base) over simulations under no fishing (F_0), recent average fishing mortality ($F_{squo} = \bar{F}_{2021-2023}$), and at the limit fishing mortality rate (F_{lim}). Spring bloom timing indices are projected under three scenarios assuming no future trend in the spring bloom timing abundance (zero trend), a trend for later timing (20% later), and a trend for earlier timing (20% earlier). Quantities shown are spawning biomass (SSB_{2053}) and recruitment (R_{2053}) at the end of the 30-year projection period, as well as mean recruitment ($\bar{R}_{2024-2053}$) and catch ($\bar{C}_{2024-2053}$) over projections. Biomass and catch units are in thousands of tonnes (kt), while recruitment is in millions (M) of fish.

Assessment Model + Index Scenario	SSB_{2053} (kt)	R_{2053} (M)	$\bar{R}_{2024-2053}$ (M)	$\bar{C}_{2024-2053}$ (kt)
F = 0, no fishing mortality				
Base	33.2 (51)	41.1 (185)	40.4 (32)	0.0 (0)
SB Timing AM + Zero trend	36.3 (30)	43.3 (86)	43.8 (15)	0.0 (0)
SB Timing AM + 20% later	31.9 (26)	36.7 (74)	40.1 (14)	0.0 (0)
SB Timing AM + 20% earlier	41.5 (37)	51.4 (100)	48.0 (17)	0.0 (0)
Recent average (status quo) fishing mortality rate				
Base	21.3 (36)	41.1 (185)	40.4 (32)	3.6 (2)
SB Timing AM + Zero trend	23.2 (22)	43.3 (86)	43.8 (15)	3.8 (1)
SB Timing AM + 20% later	20.2 (19)	36.7 (74)	40.1 (14)	3.7 (1)
SB Timing AM + 20% earlier	26.7 (27)	51.4 (100)	48.0 (17)	4.0 (1)
Limit fishing mortality rate				
Base	10.0 (19)	41.1 (185)	40.4 (32)	6.1 (3)
SB Timing AM + Zero trend	10.9 (13)	43.3 (86)	43.8 (15)	6.6 (2)
SB Timing AM + 20% later	9.5 (11)	36.7 (74)	40.1 (14)	6.3 (2)
SB Timing AM + 20% earlier	12.6 (15)	51.4 (100)	48.0 (17)	6.9 (2)

Table 6. Comparison of estimates of carrying capacity K (kt), intrinsic rate of growth r, biomass at maximum sustainable yield B_{MSY}, harvest rate producing MSY on average U_{MSY}, and survey catchability q_g and residual standard error τ_g for the late springe (splate), fall (fallcam), and early spring (spearly) campelen surveys, and the new modified campelen survey (cabs). Estimates are compared between the Witch Flounder state-space production model without environmental covariates (Base) and the original assessment (Maddock Parsons et al. 2024).

Model	K	r	B_{MSY}	U_{MSY}	B_{2021}	q_{splate}	τ_{splate}	$q_{fallcam}$	$\tau_{fallcam}$	$q_{spearly}$	$\tau_{spearly}$	q_{cabs}	τ_{cabs}
Base	136.879	0.081	68.44	0.040	27.462	0.421	0.443	0.611	0.445	0.390	0.385	0.348	0.180
Original Fit	121.500	0.122	60.75	0.061	28.430	0.358	0.411	0.545	0.359	0.438	0.413	0.453	0.418

Table 7. Maximum posterior density estimates of model parameters and derived quantities for the 3NO Witch Flounder state-space production model under the base model with no environmental covariates (Base) for process errors, and the models fit with covariates for lagged Sea Ice coverage (Sea Ice - Lag 8) and Spring Bloom Timing (SBT - Lag 3). Quantities include carrying capacity K, intrinsic rate of growth r, optimal biomass B_{MSY} (kt), limit harvest rate U_{MSY}, 2023 biomass B_{2023}, status quo harvest rate $U_{squo} = U_{2023}$, environmental covariate coefficients α, and residual process standard error $\hat{\sigma}$.

Parameter	Base	Sea Ice - Lag 8	SBT - Lag 3
K (kt)	136.879	134.794	136.021
r	0.081	0.080	0.082
B_{MSY} (kt)	68.440	67.397	68.010
$U_{lim} = U_{MSY}$	0.040	0.040	0.041
B_{2023} (kt)	29.803	16.629	29.697
U_{squo}	0.009	0.016	0.009
α	0.000	0.058	0.047
$\hat{\sigma}$	0.019	0.012	0.017
$SD(\eta)$	0.019	0.065	0.045

Table 8. Projected mean values with standard errors for 3NO Witch flounder with sea ice covariate (Sea Ice AM) and without covariate (Base) under scenarios for no fishing (U_0), recent harvest rates ($U_{squo} = U_{2023}$), and at the limit harvest rate ($U_{lim} = U_{MSY}$). Sea ice indices are projected under three scenarios assuming no future trend in sea ice extent (zero trend), increasing sea ice (20% increase), and declining sea ice (20% decline). Quantities shown are the harvest rate used in the projection U_{proj}, biomass at the end of the historical period B_{2023} and end of the projection B_{2053}, and average catch over the projection period from 2024-2053 ($\bar{C}_{2024-2053}$). Biomass and catch units are in thousands of tonnes.

Assessment Model + Index	U_{proj}	B_{2023}	B_{2053}	$\bar{C}_{2024-2053}$
U = 0, no fishing mortality				
Base	0.000	29.8	103.2 (6)	0.00 (0.00)
Sea Ice AM + Zero Trend	0.000	16.5	69.8 (28)	0.00 (0.00)
Sea Ice AM + 20% increase (more ice)	0.000	16.5	76.3 (30)	0.00 (0.00)
Sea Ice AM + 20% decline (less ice)	0.000	16.5	63.7 (26)	0.00 (0.00)
2023 (status quo) harvest rate				
Base	0.009	29.8	89.3 (6)	0.54 (0.03)
Sea Ice AM + Zero Trend	0.016	16.5	50.3 (22)	0.49 (0.12)
Sea Ice AM + 20% increase (more ice)	0.016	16.5	55.3 (24)	0.51 (0.13)
Sea Ice AM + 20% decline (less ice)	0.016	16.5	45.7 (20)	0.48 (0.12)
Limit harvest rate				
Base	0.040	29.8	50.1 (4)	1.65 (0.09)
Sea Ice AM + Zero Trend	0.038	16.5	31.2 (15)	0.85 (0.20)
Sea Ice AM + 20% increase (more ice)	0.038	16.5	34.5 (16)	0.88 (0.21)
Sea Ice AM + 20% decline (less ice)	0.038	16.5	28.2 (13)	0.82 (0.19)

Table 9. Projected mean values with standard errors for 3NO Witch flounder with spring bloom timing covariate (SB Timing AM) and without covariate (Base) under scenarios for no fishing (U_0), recent harvest rates ($U_{squo} = U_{2023}$), and at the limit harvest rate ($U_{lim} = U_{MSY}$). Spring bloom timing indices are projected under three scenarios assuming no future trend in the spring bloom timing abundance (zero trend), a trend for later timing (20% later), and a trend for earlier timing (20% earlier). Quantities shown are the harvest rate used in the projection U_{proj}, biomass at the end of the historical period B_{2023} and end of the projection B_{2053}, and average catch over the projection period from 2024-2053 ($\bar{C}_{2024-2053}$). Biomass and catch units are in thousands of tonnes.

Assessment Model + Index	U_{proj}	B_{2023}	B_{2053}	$\bar{C}_{2024-2053}$
U = 0, no fishing mortality				
Base	0.000	29.8	103.2 (6)	0.00 (0.00)
SB Timing AM + Zero Trend	0.000	29.3	107.2 (19)	0.00 (0.00)
SB Timing AM + 20% later	0.000	29.3	116.7 (20)	0.00 (0.00)
SB Timing AM + 20% earlier	0.000	29.3	98.2 (18)	0.00 (0.00)
2023 (status quo) harvest rate				
Base	0.009	29.8	89.3 (6)	0.54 (0.03)
SB Timing AM + Zero Trend	0.009	29.3	93.5 (18)	0.59 (0.08)
SB Timing AM + 20% later	0.009	29.3	102.2 (19)	0.61 (0.08)
SB Timing AM + 20% earlier	0.009	29.3	85.3 (16)	0.57 (0.07)
Limit harvest rate				
Base	0.040	29.8	50.1 (4)	1.65 (0.09)
SB Timing AM + Zero Trend	0.042	29.3	52.8 (12)	1.84 (0.25)
SB Timing AM + 20% later	0.042	29.3	58.5 (13)	1.92 (0.26)
SB Timing AM + 20% earlier	0.042	29.3	47.5 (11)	1.78 (0.24)

7. Figures

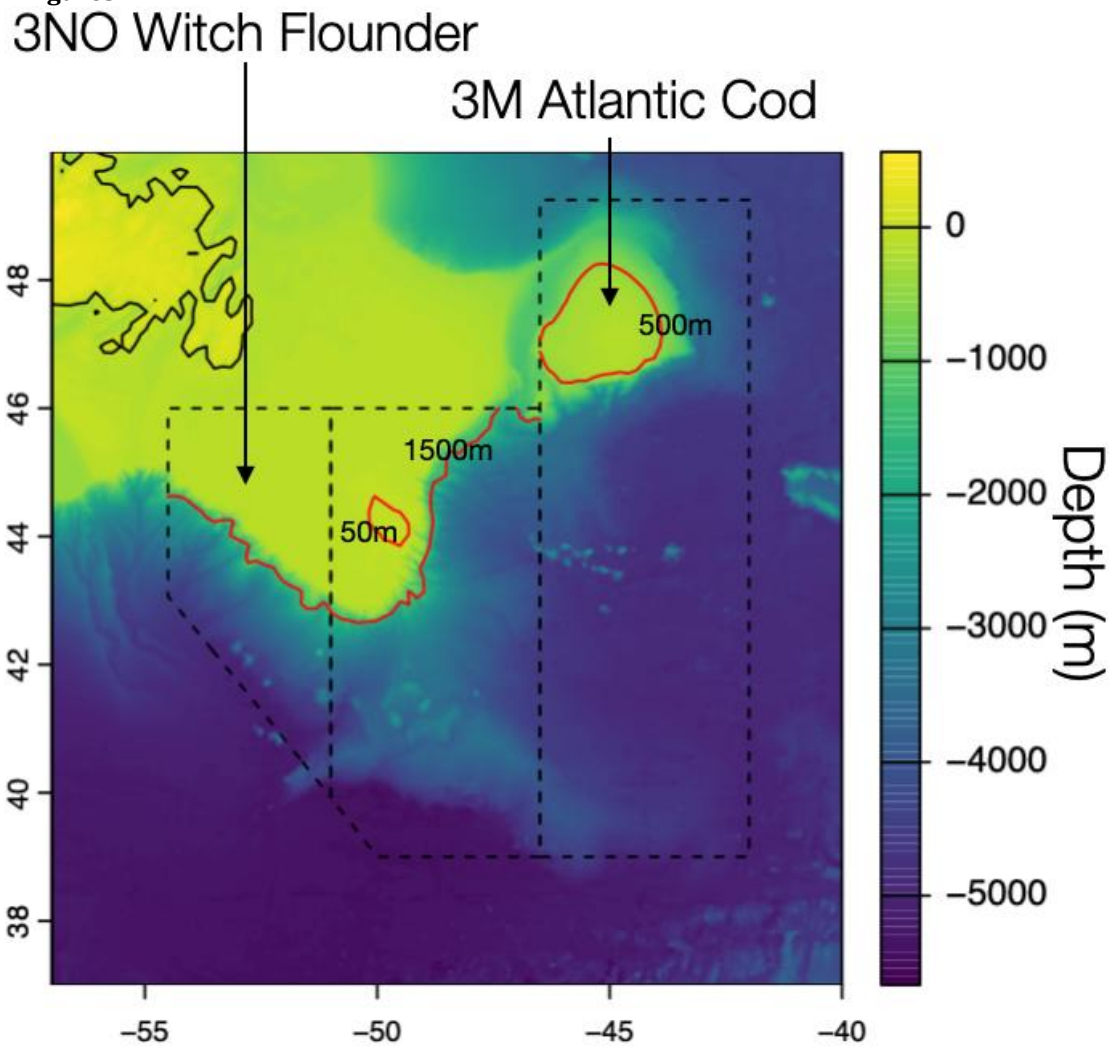

Figure 1. A map showing the habitat areas used to calculate monthly CMIP6 SST. Habitat area for Atlantic Cod includes the 100 - 500 m depth range within 3M. Habitat area for Witch Flounder includes the 50 - 1500 m depth range within 3NO. Black dashed lines show NAFO Divisions 3M, 3N, and 3O. Contour lines shown in red for 500 m in 3M, and 50 m and 1500 m in 3NO.

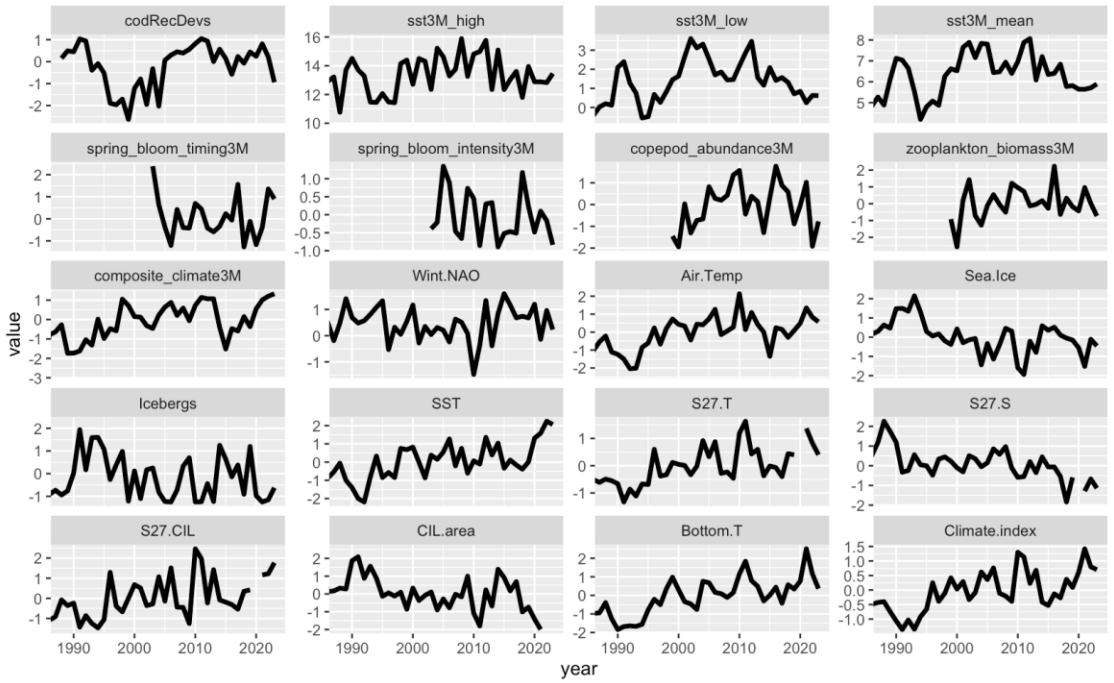

Figure 2. Time series of environmental indices in 3M used for correlation analyses, including Atlantic Cod recruitment residuals (codRecDevs in topleft).

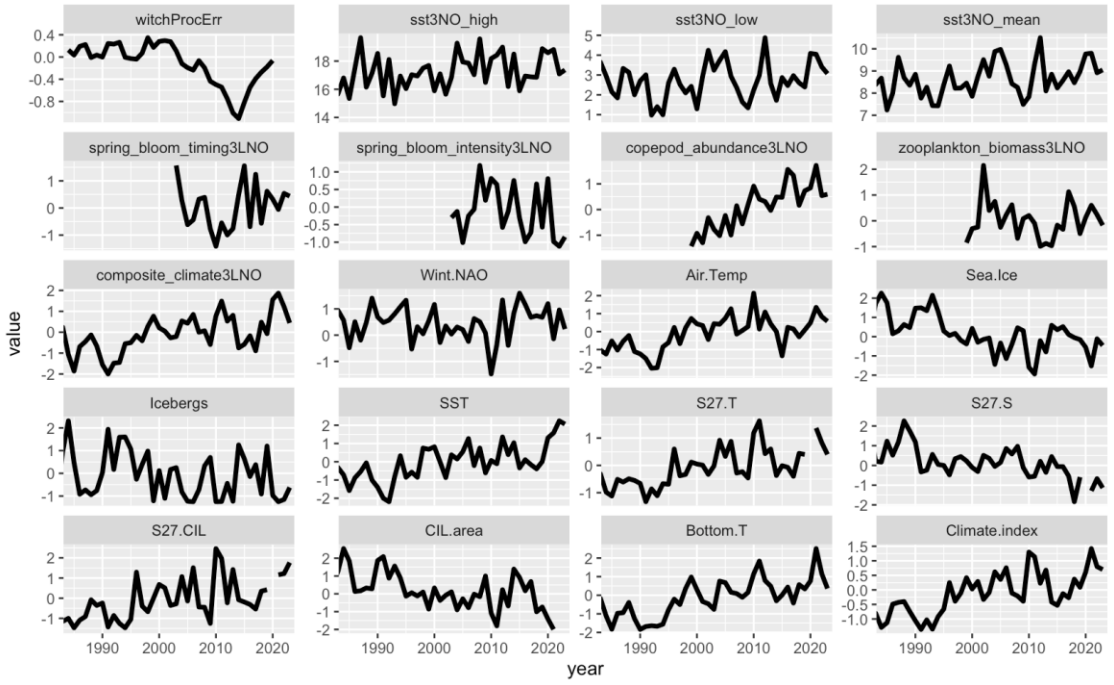

Figure 3. Time series of environmental indices in 3NO used for correlation analyses, including Witch Flounder process errors (witchProcErr in topleft).

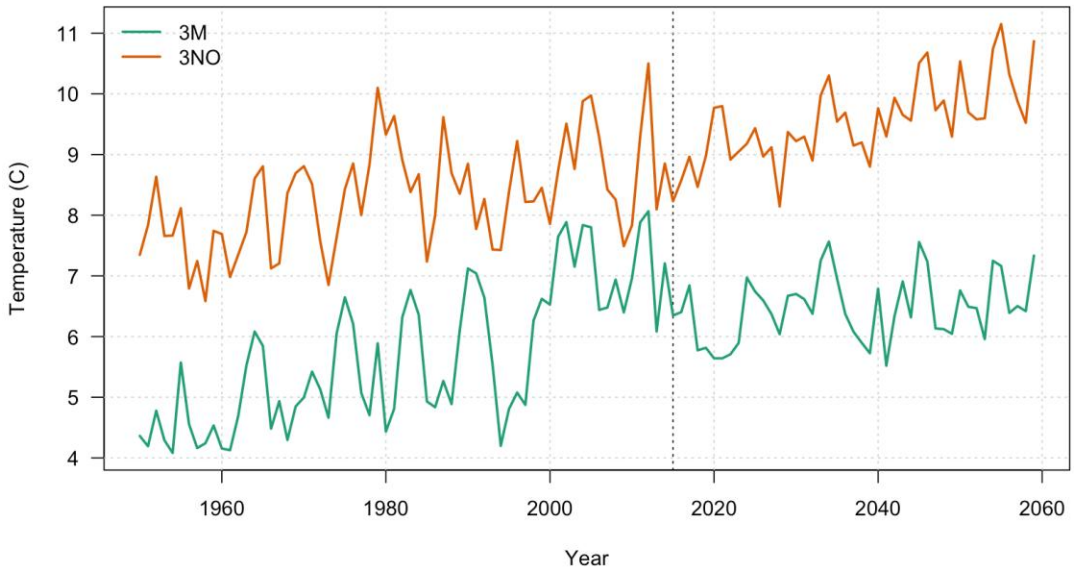

Figure 4. Time series of mean monthly SST in 3NO and 3M derived from CMIP6 historical and projection data. Projections data is shown 2015-2060, calculated as the mean from two shared socio-economic pathway scenarios (ssp245, ssp370). Dotted vertical line shows first projection year: 2015.

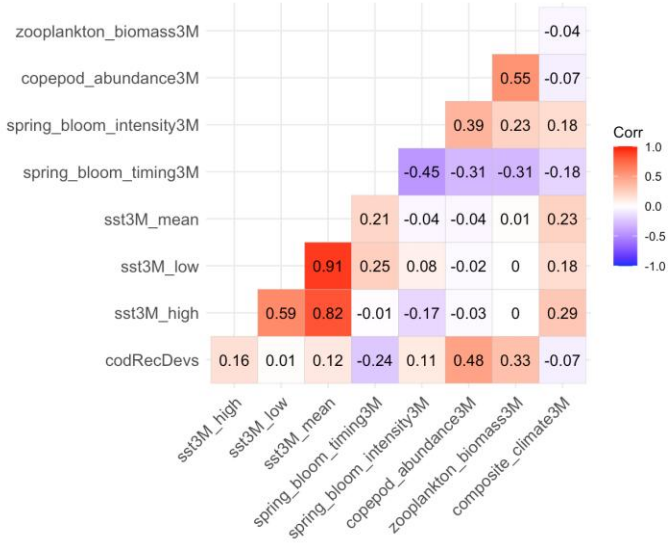

Figure 5. Pairwise correlation coefficients among Atlantic Cod recruitment deviations (codRecDevs CMIP6 SST indices, and STACFIS environmental indices.

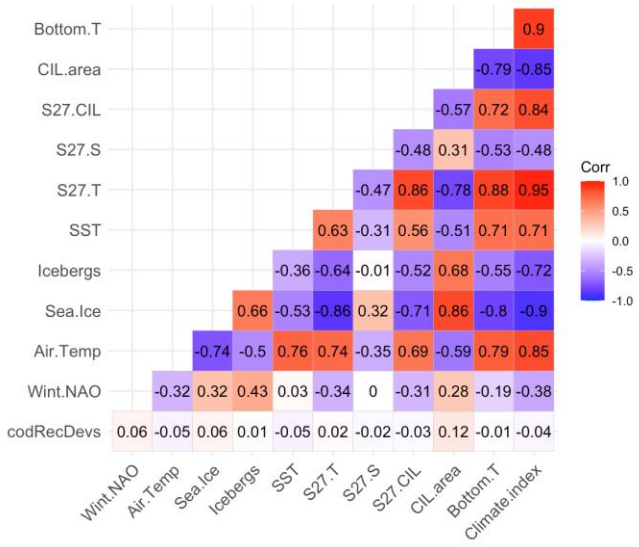

Figure 6. Pairwise correlation coefficients among Atlantic Cod recruitment deviations (codRecDevs) and NL climate indices (Cyr and Galbraith 2020; 2023).

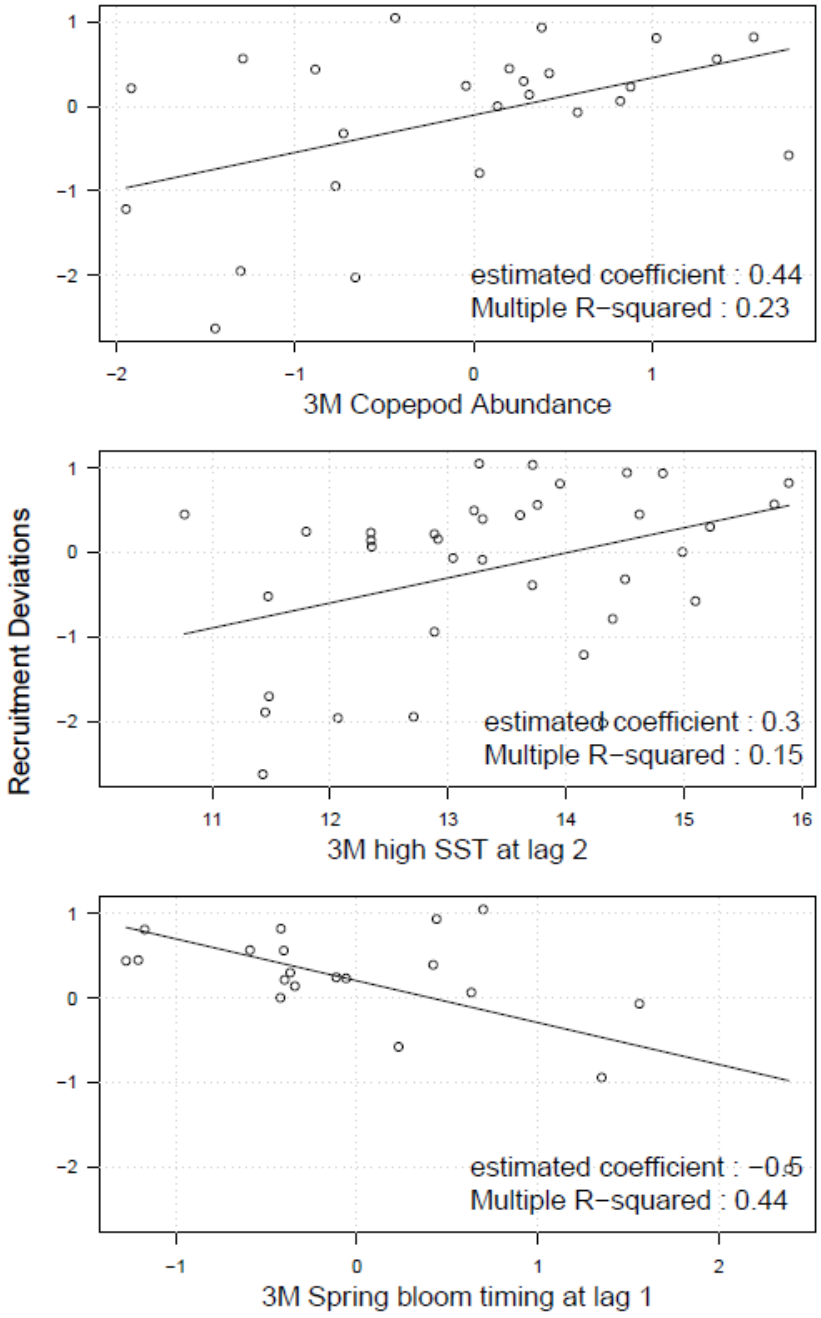

Figure 7. Linear regression analysis results between Atlantic Cod recruitment deviations (recDevs) and selected environmental indices.

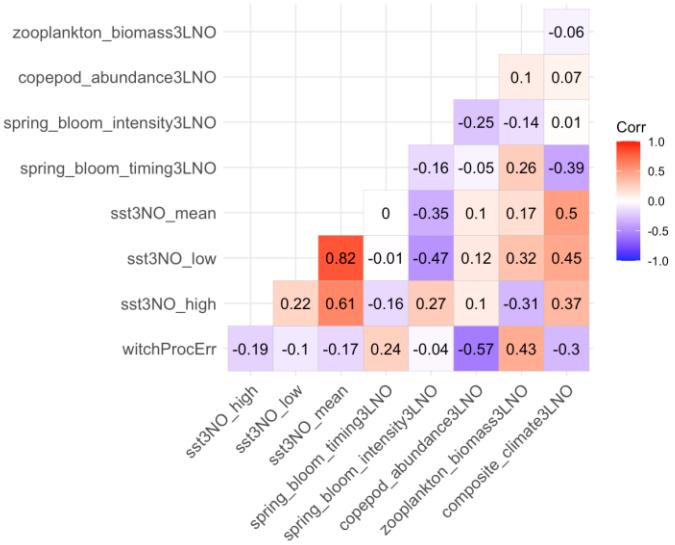

Figure 8. Pairwise correlation coefficients among Witch Flounder process errors, CMIP6 SST indices, and STACFIS environmental indices.

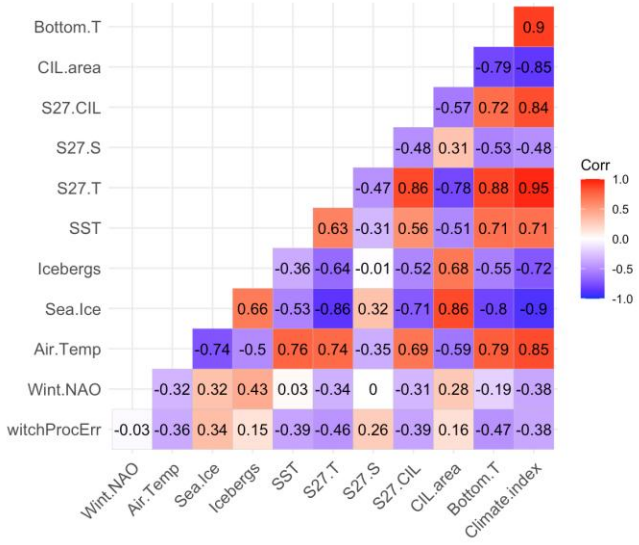

Figure 9. Pairwise correlation coefficients among Witch Flounder process errors (witchProcErr) and NL climate indices (Cyr and Galbraith 2020; 2023).

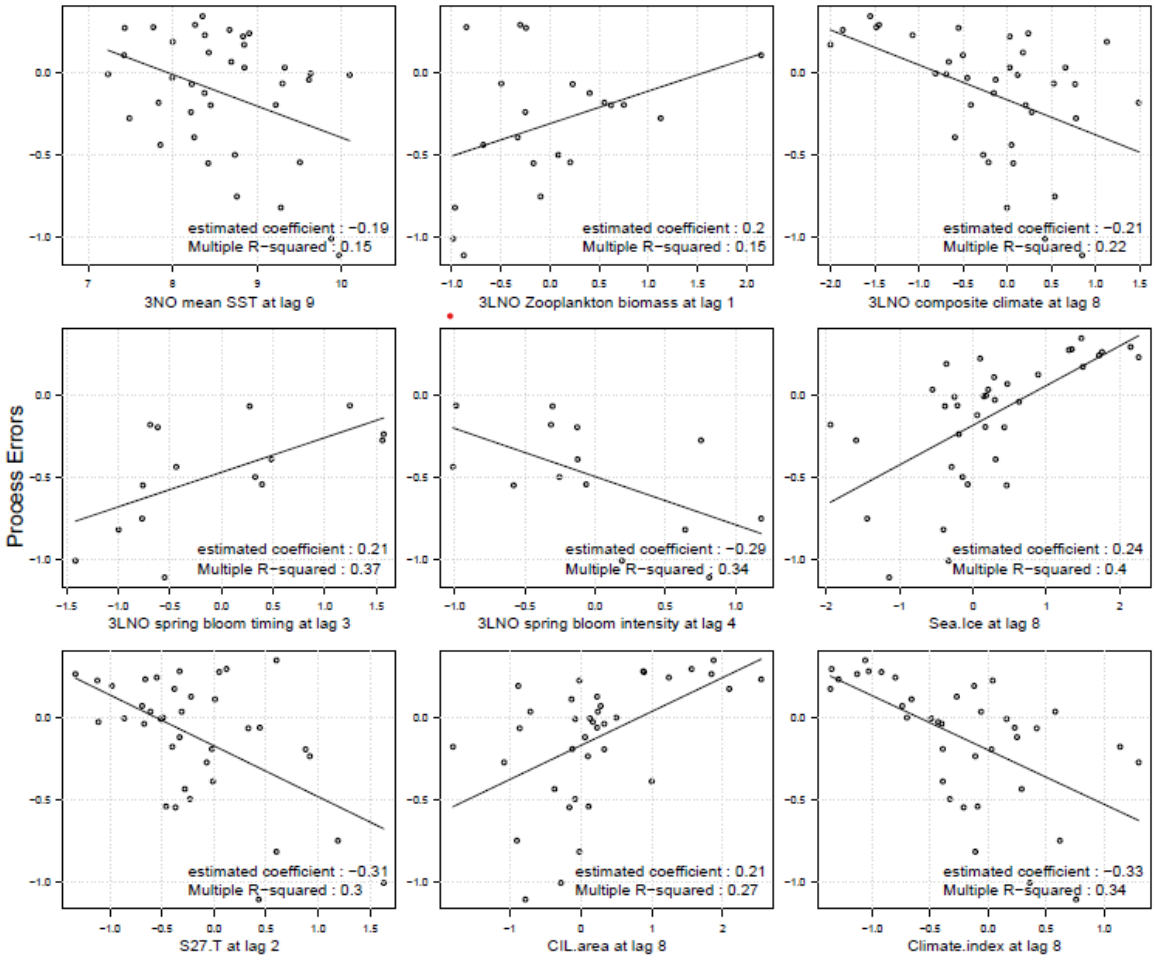

Figure 10. Linear regression analysis results between Witch Flounder process errors (procErrs) and selected environmental indices.

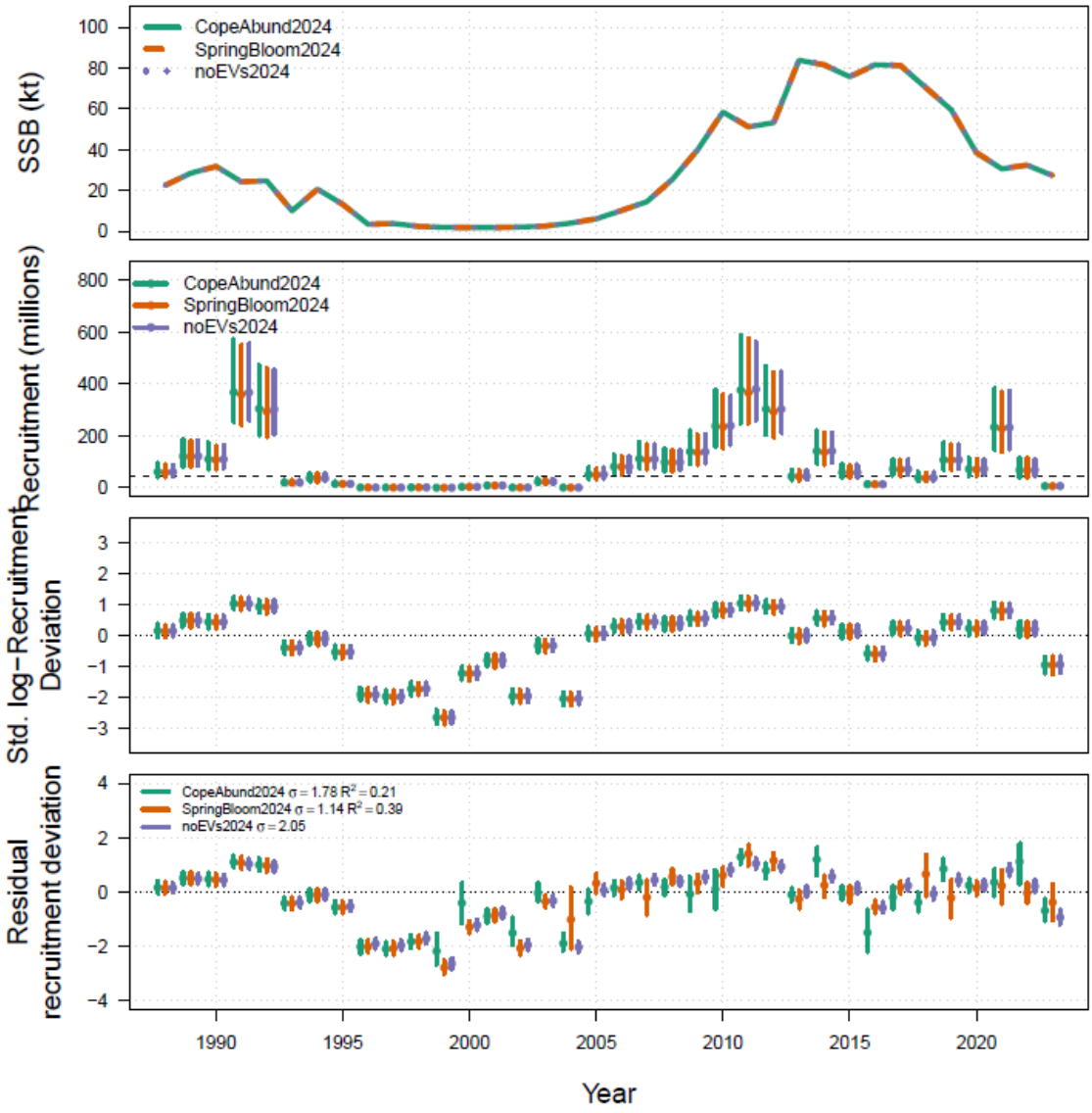

Figure 11. Comparison of Atlantic Cod model fits with and without environmental covariates for spawning biomass (SSB, top panel), recruitments (2nd panel), total recruitment process errors (3rd panel), and the random component of recruitment process errors (4th panel). The total recruitment process errors are split into environmental and random components for models with environmental covariates.

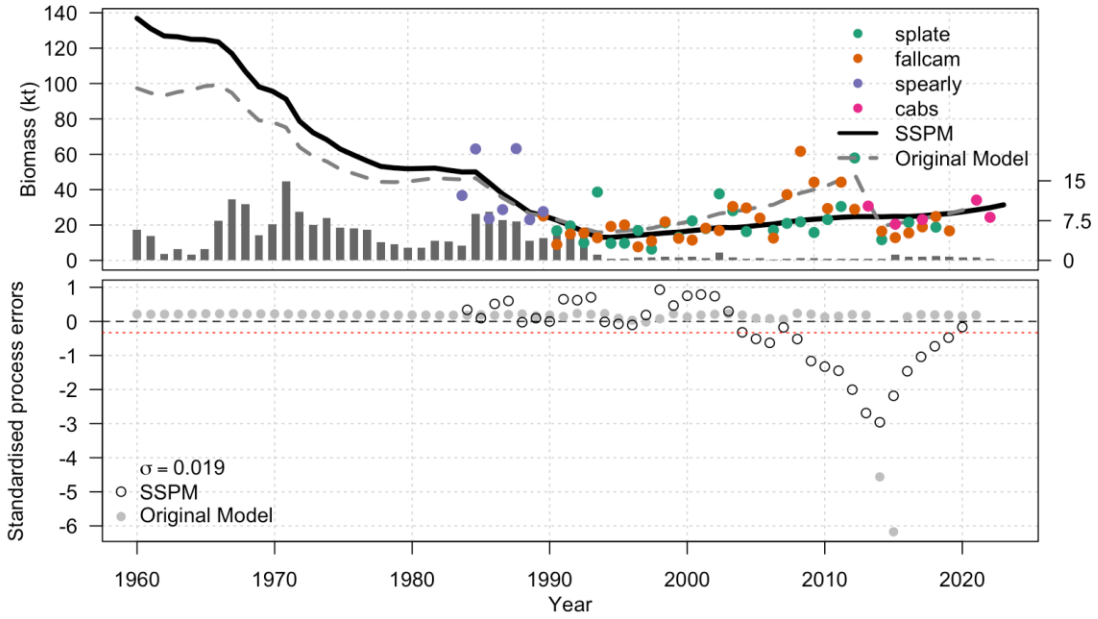

Figure 12. Top panel: 3NO Witch Flounder assessment models of exploitable biomass for SSPM model (thick line) and original model (dashed grey line) from Maddock Parsons et al. 2024 when fit to legal sized landings (bars) and biomass indices (points). Bottom panel: 3NO Witch Flounder SSPM and original model standardised process error deviations. Mean process error for SSPM is indicated by the red horizontal line.

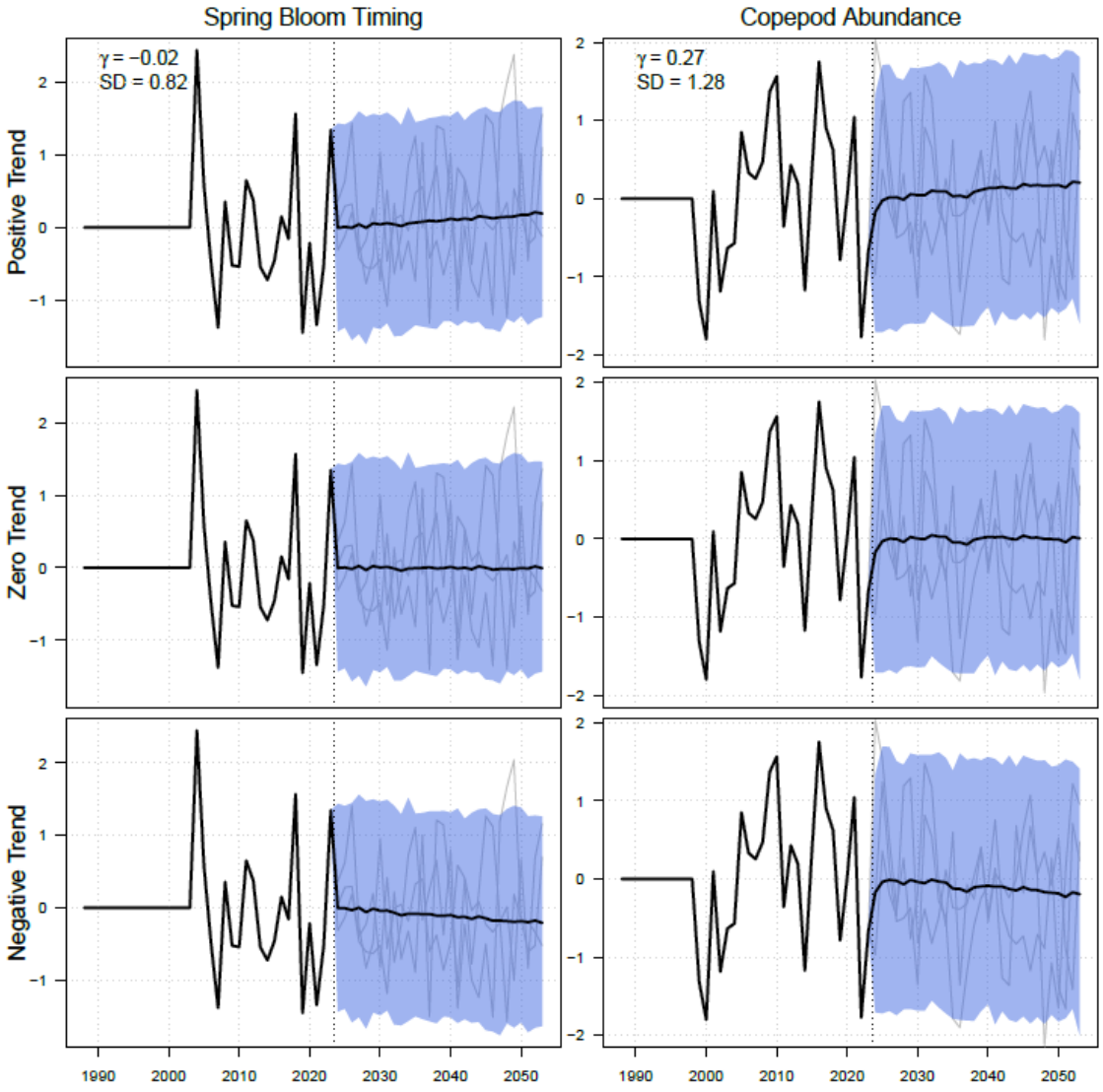

Figure 13. Comparison of simulation envelopes for the projected environmental variables used in the Cod models. Shaded regions show the central 95% of the simulated model states in the projection, black lines show the mean, and grey lines show three random traces for each model. γ is the autocorrelation coefficient of the environmental index and SD is the standard deviation of the difference between successive environmental index values.

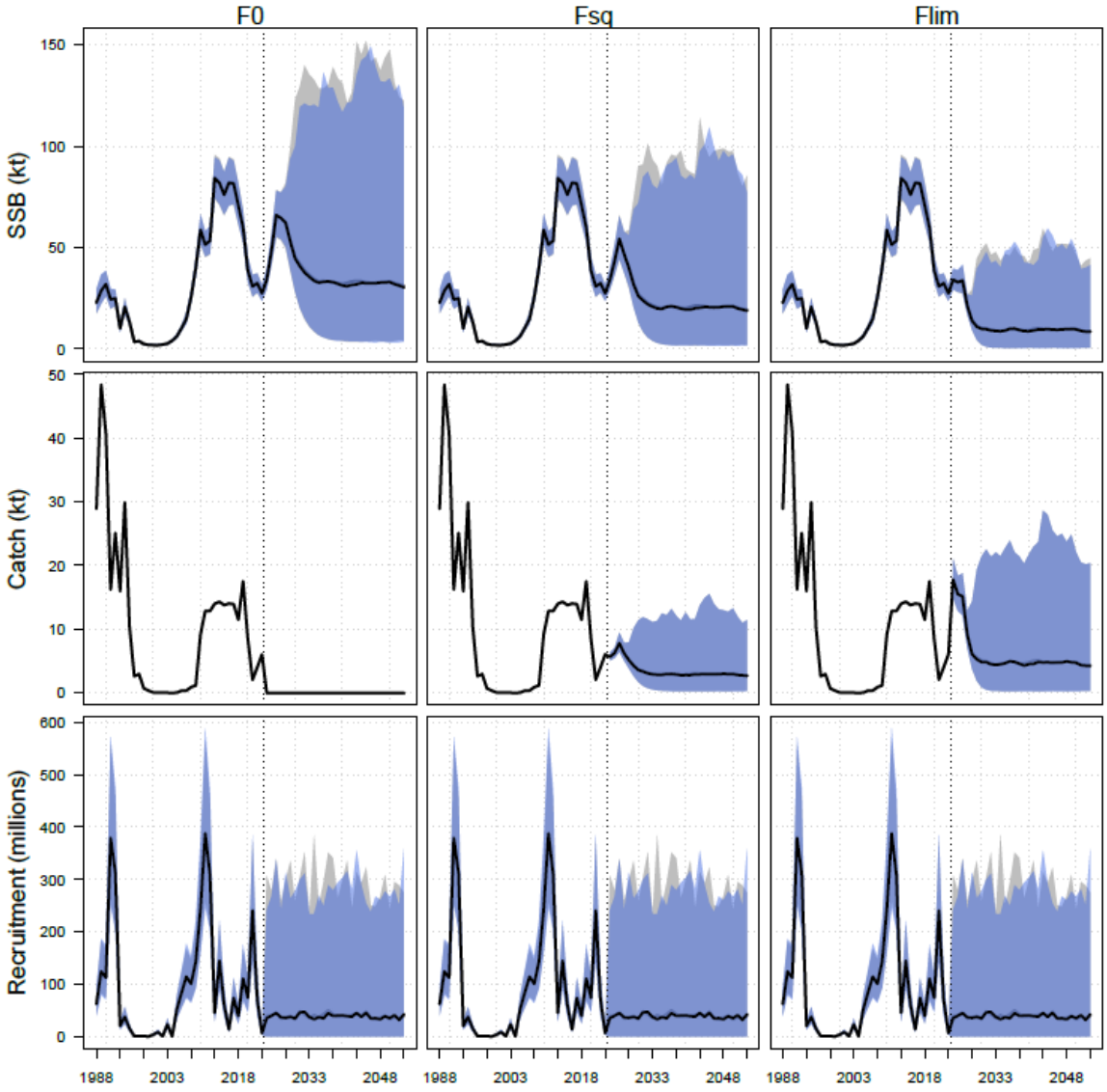

Figure 14. Comparison of simulation envelopes for the base model (grey shaded region, grey mean line) and the model fit to the copepod abundance index with zero projected trend in the index (blue shaded 95% and black mean lines). Time series of biomass (top), catch (middle row), and recruitment (bottom) over the model history and projection period are shown under scenarios for no fishing (F0, left hand column), recent average fishing mortality (Fsquo, middle column), and fishing at the fishing mortality limit reference point (Flim, right hand column). Shaded regions show the central 95% of parameter uncertainty under the bayes posterior in the history, and the central 95% of the simulated model states in the projection.

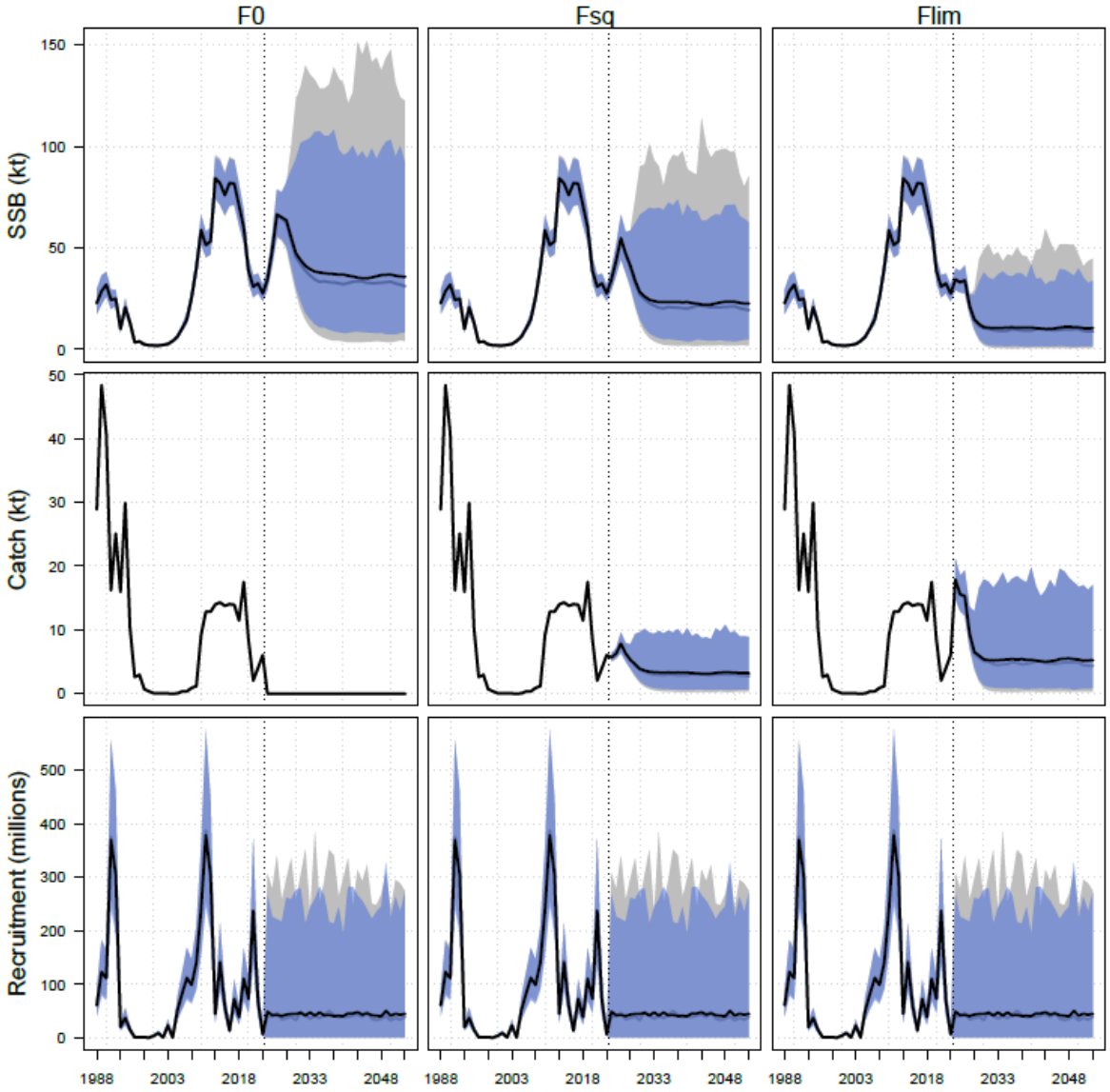

Figure 15. Comparison of simulation envelopes for the base model (grey shaded region, grey mean line) and the model fit to the spring bloom timing index with zero projected trend in the index (blue shaded 95% and black mean lines). Time series of biomass (top), catch (middle row), and recruitment (bottom) over the model history and projection period are shown under scenarios for no fishing (F0, left hand column), recent average fishing mortality (Fsquo, middle column), and fishing at the fishing mortality limit reference point (Flim, right hand column). Shaded regions show the central 95% of parameter uncertainty under the bayes posterior in the history, and the central 95% of the simulated model states in the projection.

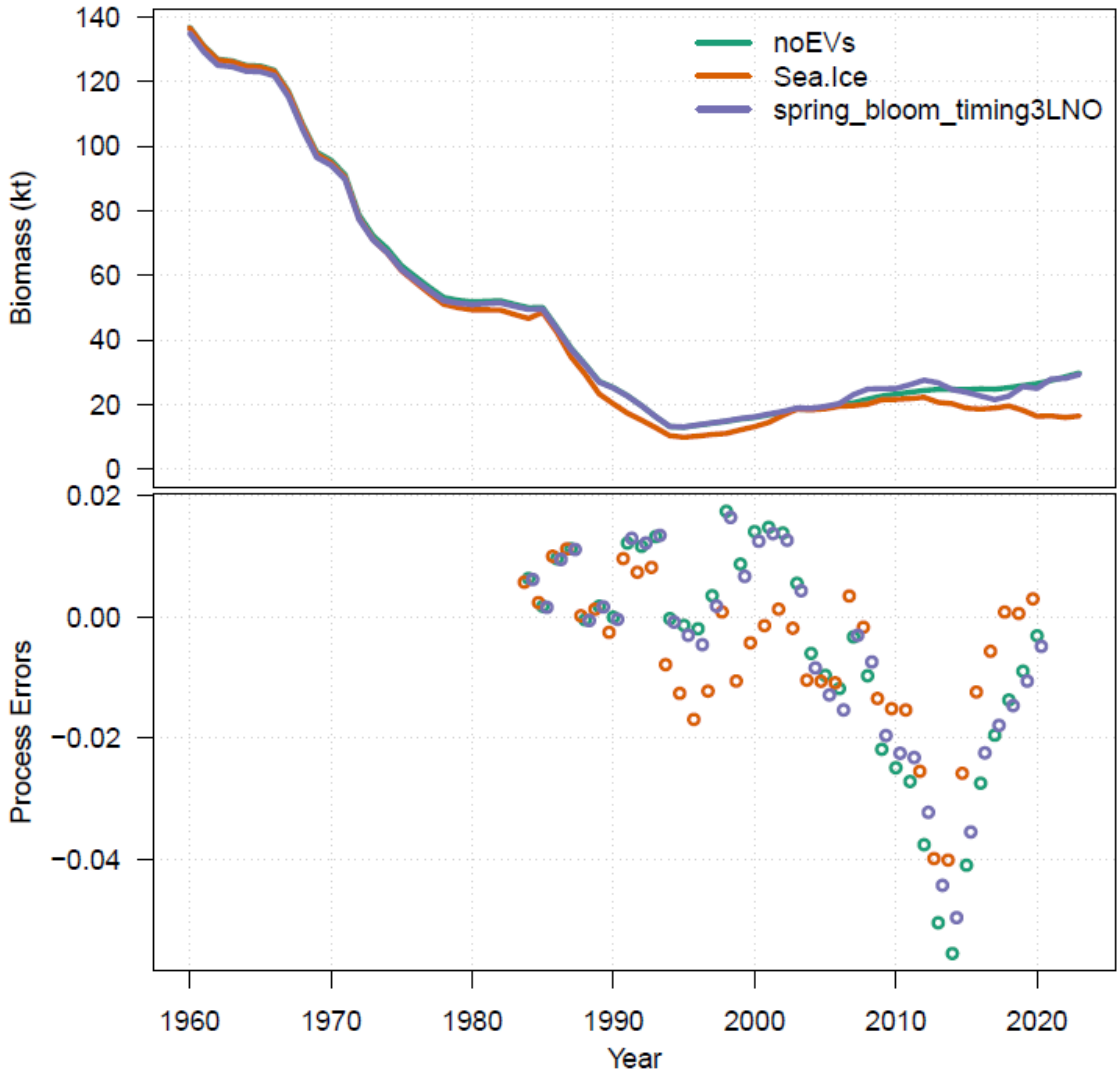

Figure 16. 3NO Witch Flounder maximum posterior density estimates of biomass (top) and process errors (bottom) under the base model without environmental covariates and models with sea ice and spring bloom timing process error covariates.

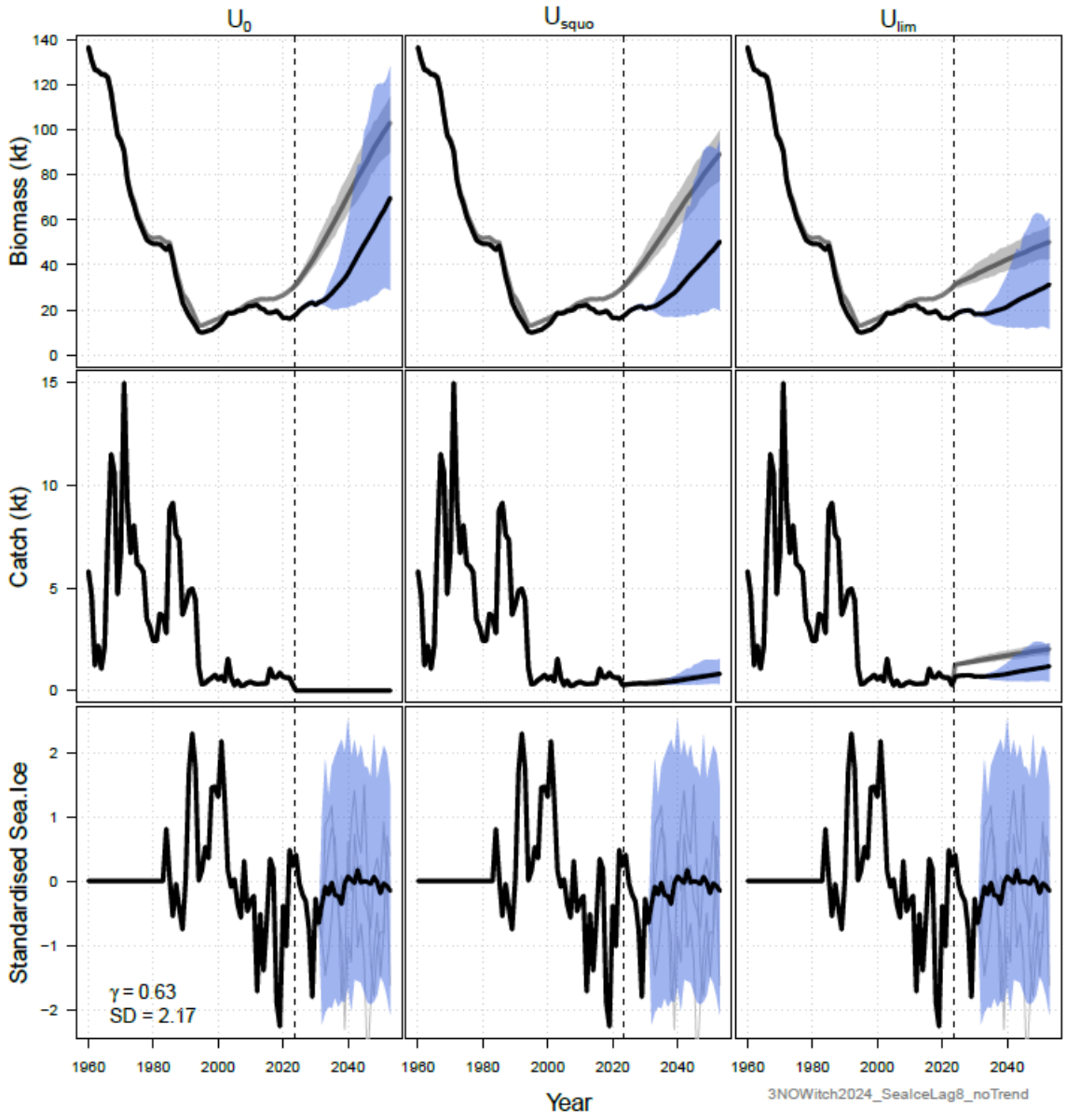

Figure 17. Comparison of simulation envelopes for the base model (grey shaded region, grey mean line) and the model fit to lagged sea ice with zero projected trend in the index (blue shaded 95% and black mean lines). Time series are shown for biomass (top), catch (middle row), and standardized Ice index (bottom) over the model history and projection period under scenarios for no fishing (U0, left hand column), recent average fishing mortality (Usquo, middle column), and fishing at the fishing mortality limit reference point (Ulim, right hand column). Shaded regions show the central 95% of parameter uncertainty under the bayes posterior in the history, and the central 95% of the simulated model states in the projection. γ is the autocorrelation coefficient of the environmental index and SD is the standard deviation of the difference between successive environmental index values.

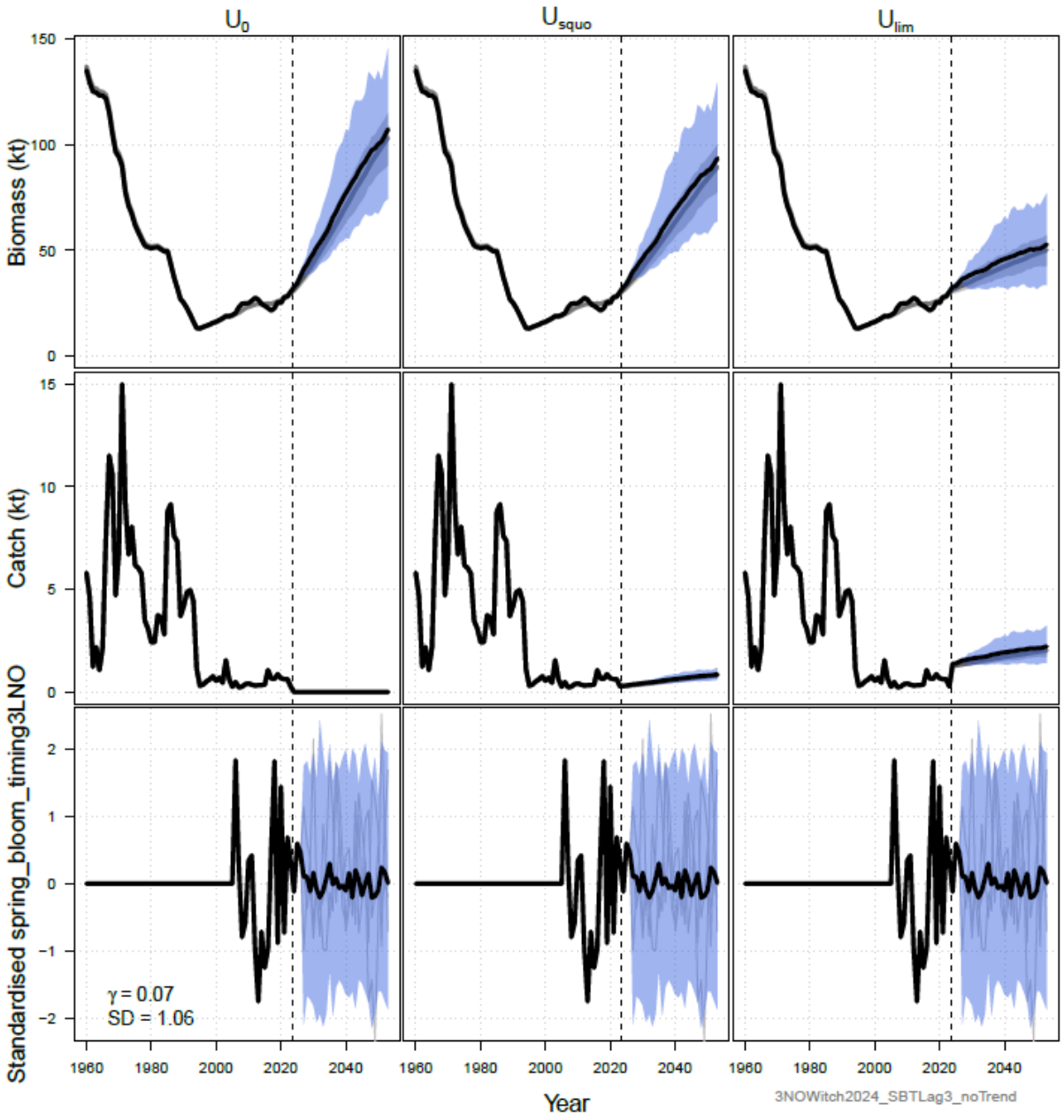

Figure 18. Comparison of simulation envelopes for the base model (grey shaded region, grey mean line) and the model fit to lagged spring bloom timing with zero projected trend in the index (blue shaded 95% and black mean lines). Time series are shown for biomass (top), catch (middle row), and standardized spring bloom timing index (bottom) over the model history and projection period under scenarios for no fishing (U0, left hand column), recent average fishing mortality (Usquo, middle column), and fishing at the fishing mortality limit reference point (Ulim, right hand column). Shaded regions show the central 95% of parameter uncertainty under the bayes posterior in the history, and the central 95% of the simulated model states in the projection. γ is the autocorrelation coefficient of the environmental index and SD is the standard deviation of the difference between successive environmental index values.

A. Appendices

A.1. State Space Production Model for 3NO Witch Flounder

A.1.1. Model specification

3NO Witch Flounder (*Glyptocephalus cynoglossus*) biomass was modeled using a state-space surplus production model (SSPM) of the form

$$B_{t+1} = \left(B_t + r \cdot B_t\left(1 - \frac{B_t}{K}\right) - C_t\right)e^{\eta_t}$$

where B_t is the recruited Witch Flounder biomass the start of year t, r is the intrinsic growth rate of the population, K is the carrying capacity, C_t is total catch in thousands of tonnes in year t, and η_t are annual process errors. Witch flounder was assumed to be initialised in an unfished state, i.e., $B_{1960} = K$. The SSPM was specified in Template Model Builder (Kristensen et al. 2016).

Recruited biomass indices for survey $g \in \{1, \ldots, 4\}$ are assumed to be log-Normally distributed as

$$I_{t,g} \sim \log N\left(q_g B_t, \tau_g\right)$$

where q_g is survey catchability, and τ_g is the precision for survey index g. The inverse of catchability and precision both follow a Gamma(1,1) prior (Table 8.1).

Maximum posterior density estimates of model quantities were found by optimising the model's objective function with respect to the parameters r, K, q_g, τ_g, and annual process error terms η_t. The objective function was the posterior negative log-density, which was the sum of log-likelihood functions for survey biomass indices, and log-prior density functions (Table 8.1).

Likelihood functions and prior density functions were weighted for all surveys. The weighting w_g was 1 for the late Spring (splate), fall (fallcam), and early spring (spearly) campelen surveys, but 0.3 for the new modified campelen survey (cabs). Higher weightings on the cabs survey produced non convergent model parameters (non-finite standard errors).

Table A.1. Notation for the generalized logistic population dynamics model for marine mammals.

Symbol	Description
	Indices and index ranges
T	Year in which stock assessment is performed
t	Year, where $t = t_1, ..., T$
g	Survey index g for splate ($g = 1$), fallcam ($g = 2$), spearly ($g = 3$), and cab ($g = 4$)
n_g	Number of non-missing observations for the index g
	Data
C_t	Catch in biomass removed during year t
$I_{t,g}$	Survey biomass index in yera g
w_g	Weighting for index likelihood and priors for gear g
	Leading life history parameters
K	Carrying capacity
r	Intrinsic growth rate
	Observation model
q_g	Catchability coefficient for survey index g
τ_g	Survey precision
	Process errors
ω_t	Random component of biomass process errors
	State variables
B_t	Biomass at the beginning of year t
	Statistical model
	Data Likelihood
	$I_{t,g} \sim \log -N(q_g B_t, \tau)$
	Prior distributions
	$r \sim \log N(0.17, 3.252)$
	$K \sim \log N(0.17, 3.252)$

Table A.1. Notation for the generalized logistic population dynamics model for marine mammals. (continued)

Symbol	Description
	$1/q_g \sim \text{Gamma}(1,1)$
	$1/\tau_g \sim \text{Gamma}(1,1)$

A.1.2 Goodness of fit

Standard goodness of fit metrics for the SSPM on 3NO Witch Flounder data was acceptable. Estimated parameters all had gradients less than 10^{-4} in magnitude, and the coefficients of variation (CVs) were low for leading model parameters. Catchability, survey precision, and process error terms had higher CVs, but all were within acceptable levels (Table 8.2).

Survey biomass residuals were close to unbiased. Mean survey index residuals ranged from 0.15 to 0.28 standard errors (Figure 8.1), with larger biases observed in indices with fewer data points.

Process error terms had an effective standard error of 0.019, and a mean deviation of about -0.2 standard errors (Figure 8.2). The negative mean deviation is driven by the string of negative process errors from 2004 - 2020, which by eye look highly auto-correlated. Such behaviour in process errors usually aliases some unmodeled process that is affecting stock productivity, indicating that a re-specification of the model to capture that process may be warranted.

A comparison of prior distributions and maximum posterior density estimates (MPDEs) indicates that the data appear to be more influential than the priors for K, r, and q_g, but are perhaps influential on τ_g values (Figures 8.3 and 8.4). MPDEs for K, r, and q_g are often far from the prior mean, and sometimes in areas of relatively low prior density. While τ_g estimates are similarly far from the prior mean, they are often towards the higher prior density regions.

Table A.2. SSPM leading parameters estimates, standard errors, gradients, and CVs.

Parameter	Estimate	SE	CV	Gradient
lnB0	4.9191	0.0647	0.004	5.0e-06
lnr	-2.5192	0.1791	0.032	7.2e-05
lnq_g	-0.8644	0.2590	0.067	-2.9e-05
lnq_g	-0.4922	0.2564	0.066	4.5e-06
lnq_g	-0.9414	0.1701	0.029	-6.2e-06
lnq_g	-1.0542	0.3188	0.102	1.6e-05
lntauObs_g	-0.8140	0.1426	0.020	-3.5e-06
lntauObs_g	-0.8097	0.1412	0.020	-9.5e-06
lntauObs_g	-0.9543	0.2641	0.070	-1.3e-06
lntauObs_g	-1.7158	0.5880	0.356	-9.0e-07
lnOmega_t	0.1267	0.9892	1.267	-1.3e-06
lnOmega_t	0.0350	0.9867	1.257	-1.2e-06
lnOmega_t	0.1920	0.9900	1.270	-1.0e-06
lnOmega_t	0.2247	0.9927	1.281	-8.0e-07

Parameter	Estimate	SE	CV	Gradient
lnOmega_t	-0.0095	0.9914	1.276	-8.0e-07
lnOmega_t	0.0351	0.9924	1.280	-7.0e-07
lnOmega_t	-0.0011	0.9906	1.273	-6.0e-07
lnOmega_t	0.2433	0.9879	1.262	-4.0e-07
lnOmega_t	0.2323	0.9880	1.262	-3.0e-07
lnOmega_t	0.2644	0.9892	1.267	-1.0e-07
lnOmega_t	-0.0057	0.9866	1.257	0.0e+00
lnOmega_t	-0.0279	0.9826	1.241	2.0e-07
lnOmega_t	-0.0390	0.9813	1.236	4.0e-07
lnOmega_t	0.0699	0.9800	1.231	4.0e-07
lnOmega_t	0.3481	0.9814	1.236	5.0e-07
lnOmega_t	0.1741	0.9801	1.231	6.0e-07
lnOmega_t	0.2812	0.9805	1.233	6.0e-07
lnOmega_t	0.2952	0.9806	1.233	5.0e-07
lnOmega_t	0.2766	0.9799	1.230	4.0e-07
lnOmega_t	0.1109	0.9818	1.238	2.0e-07
lnOmega_t	-0.1202	0.9809	1.234	1.0e-07
lnOmega_t	-0.1924	0.9790	1.227	0.0e+00
lnOmega_t	-0.2363	0.9790	1.227	-1.0e-07
lnOmega_t	-0.0660	0.9784	1.225	-4.0e-07
lnOmega_t	-0.1941	0.9763	1.217	-4.0e-07
lnOmega_t	-0.4361	0.9763	1.217	-5.0e-07
lnOmega_t	-0.4971	0.9784	1.225	-5.0e-07
lnOmega_t	-0.5422	0.9791	1.228	-6.0e-07
lnOmega_t	-0.7506	0.9836	1.245	-6.0e-07
lnOmega_t	-1.0079	0.9889	1.266	-5.0e-07
lnOmega_t	-1.1090	0.9891	1.267	-8.0e-07
lnOmega_t	-0.8182	0.9851	1.251	-6.0e-07
lnOmega_t	-0.5478	0.9755	1.214	-9.0e-07
lnOmega_t	-0.3897	0.9766	1.218	-5.0e-07
lnOmega_t	-0.2738	0.9780	1.223	-6.0e-07
lnOmega_t	-0.1789	0.9838	1.246	-2.0e-07
lnOmega_t	-0.0622	0.9877	1.261	0.0e+00

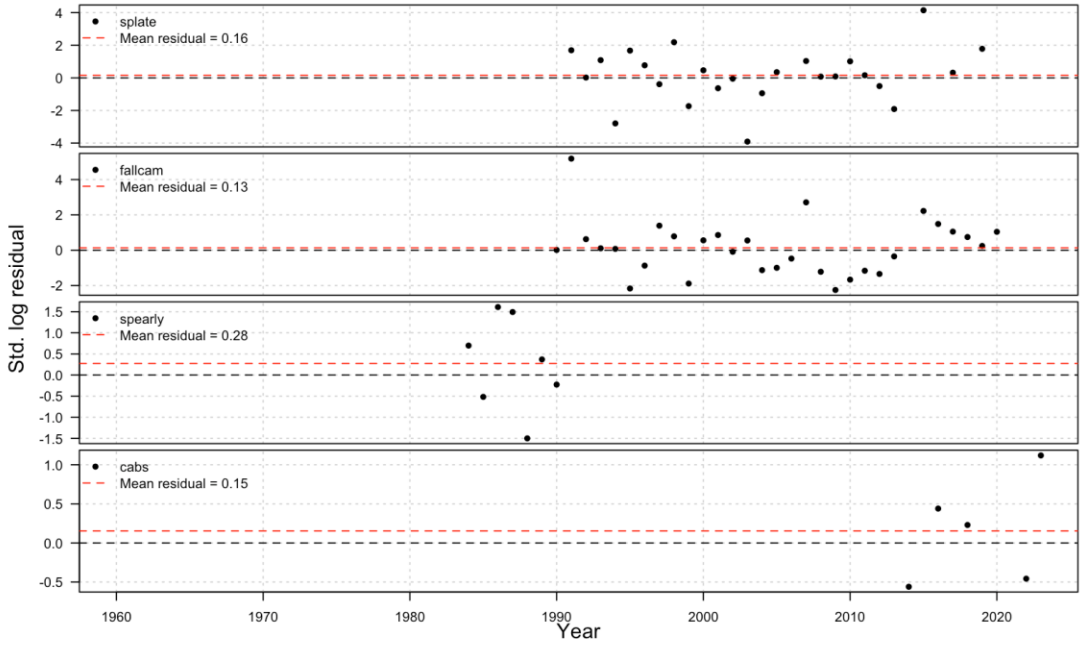

Figure A.1. 3NO Witch SSPM standardised stock index log-residuals. Red lines show mean residual error.

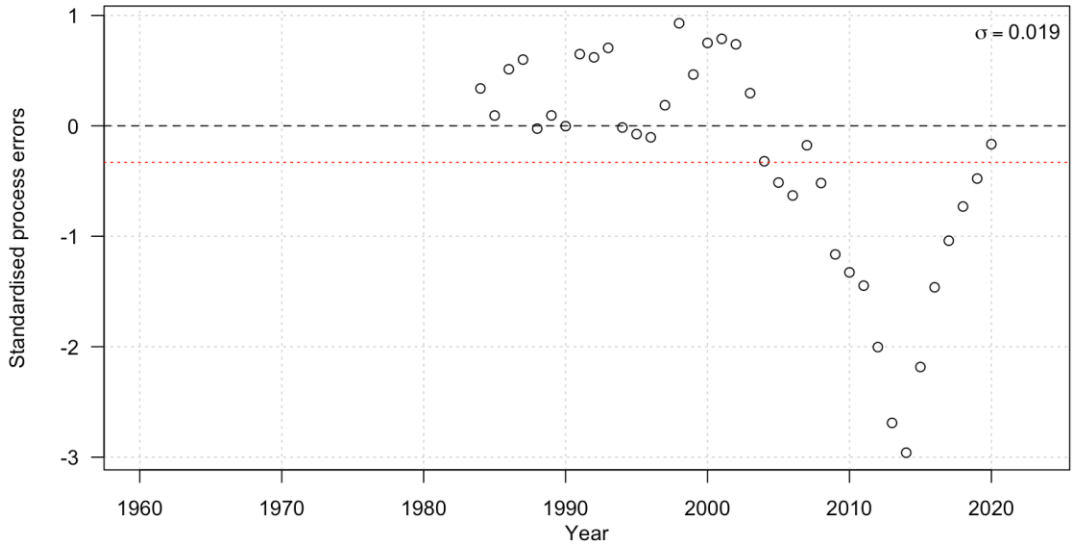

Figure A.2. 3NO Witch SSPM standardised process error deviations. Mean process error is indicated by the red horizontal line.

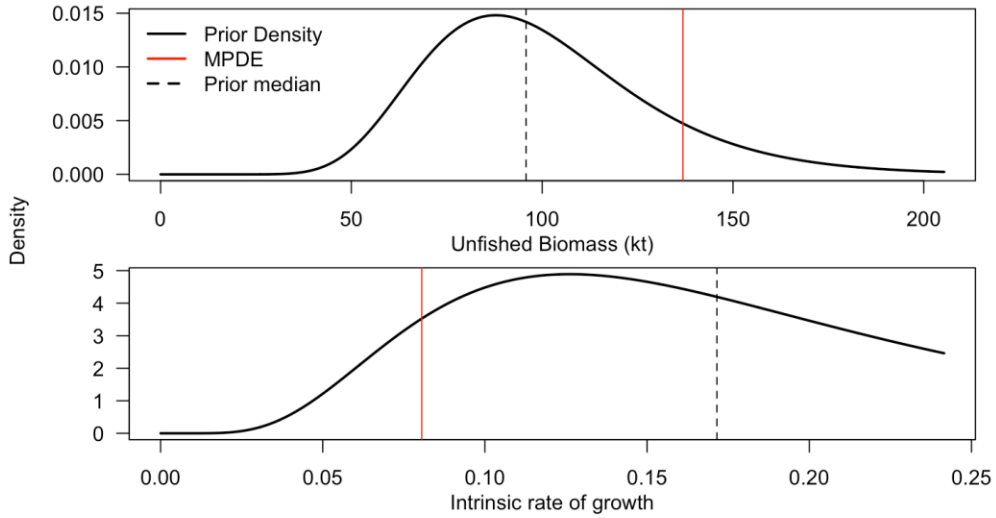

Figure A.3. Comparison of unfished biomass (top) and intrinsic rate of growth (bottom) estimates (red vertical lines) to their prior densities (black curve) and prior mean values (black vertical dashed line).

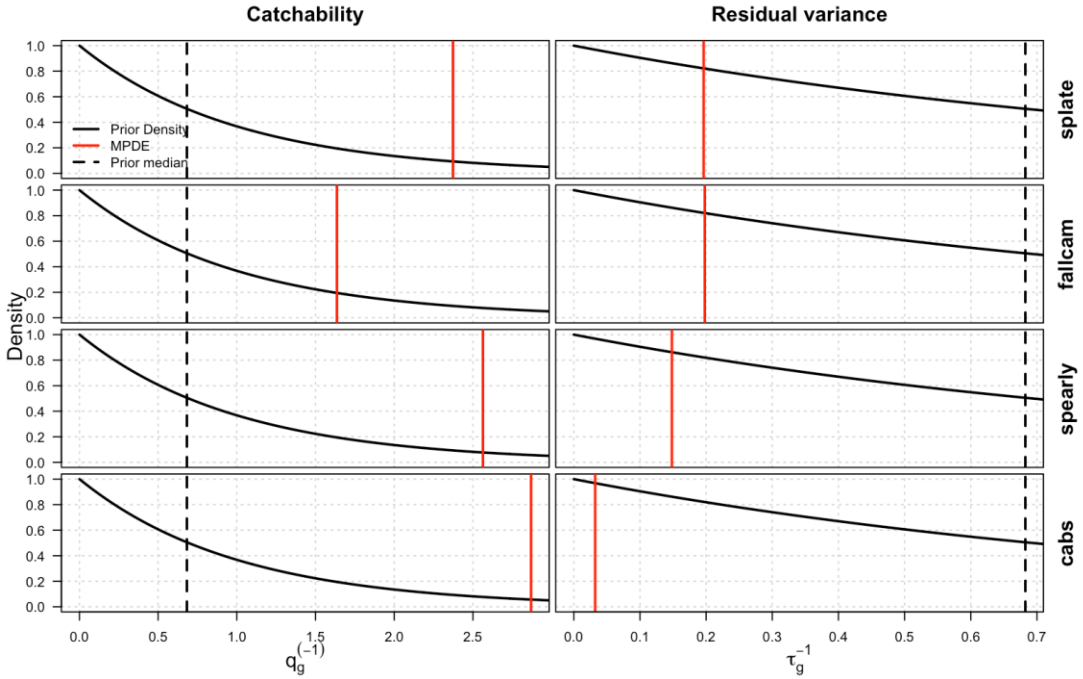

Figure A.4. Comparison of catchability (left) and stock index residual variance (right) estimates (red vertical lines) to their prior densities (black curve) and prior mean values (black vertical dashed line) for each index series.

A.1.3 Future work

The substitute SSPM model may require reparameterisation if it is to be adopted as the new 3NO Witch Flounder stock assessment model. Under the current parameterisation, we could not sample an acceptable Bayes posterior because there were a small number of so-called divergent transitions during sampling. Divergent transitions are an error that occurs during Hamiltonian Monte Carlo sampling when the discrete path taken by the sampler (a series steps) differs substantially from the continuous path predicted by the proposal distribution of the model (Monnahan 2024), and are often associated with parts of the objective function that have very high gradients. Divergent transitions indicate that a portion of the posterior was unable to be sampled, and therefore model estimates and their uncertainty are probably biased. Divergent transitions are common in state-space surplus production models, as large negative process errors may drive biomass to be lower than catch. The usual solution is to set biomass to a minimum value and add a penalty function that increases the gradient that that point, thereby causing the divergent transitions (Best and Punt 2020).

A.2 Additional model projection results

A.2.1 3M Cod

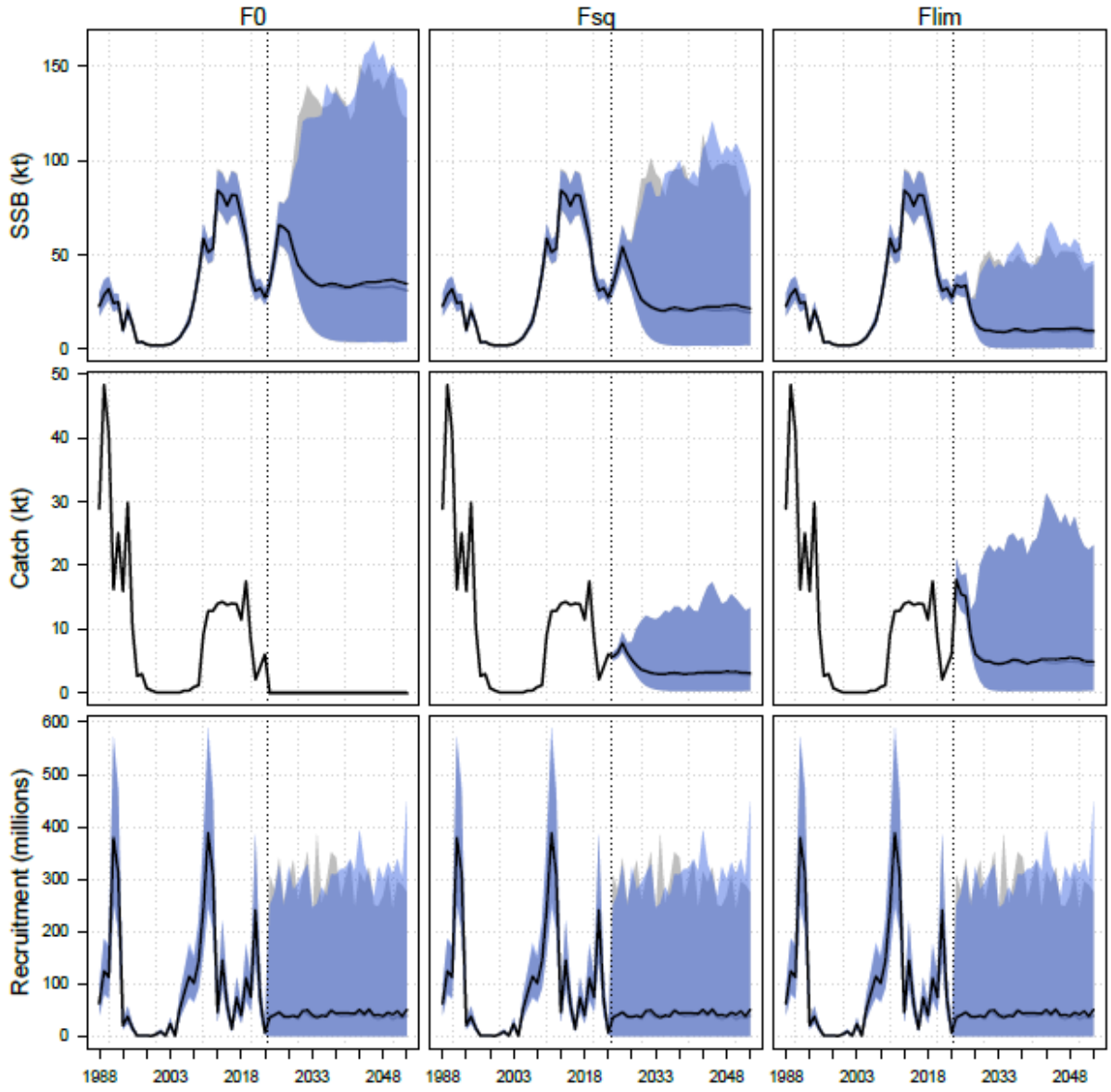

Figure A.5. Comparison of simulation envelopes for the base model (grey shaded region, grey mean line) and the model fit to the copepod abundance index with positive projected trend in the index (blue shaded 95% and black mean lines), showing biomass (top), catch (middle row), and recruitment (bottom) over the model history and projection period under no fishing (F0, left hand column), recent average fishing mortality (Fsquo, middle column), and fishing at the fishing mortality limit reference point (Flim, right hand column). Shaded regions show the central 95% of parameter uncertainty under the bayes posterior in the history, and the central 95% of the simulated model states in the projection.

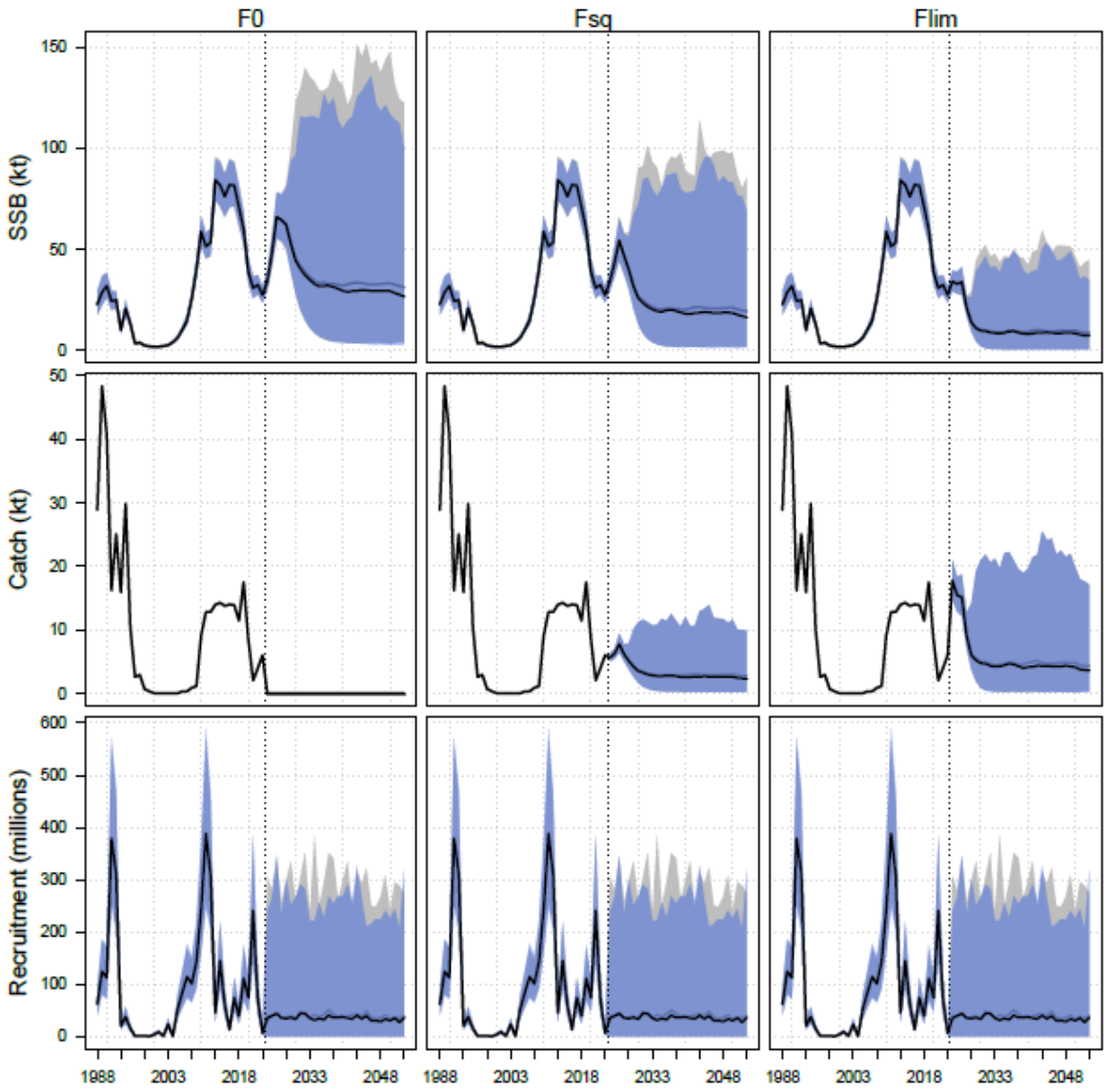

Figure A.6. Comparison of simulation envelopes for the base model (grey shaded region, grey mean line) and the model fit to the copepod abundance index with a negative projected trend in the index (blue shaded 95% and black mean lines), showing biomass (top), catch (middle row), and recruitment (bottom) over the model history and projection period under no fishing (F0, left hand column), recent average fishing mortality (Fsquo, middle column), and fishing at the fishing mortality limit reference point (Flim, right hand column). Shaded regions show the central 95% of parameter uncertainty under the bayes posterior in the history, and the central 95% of the simulated model states in the projection.

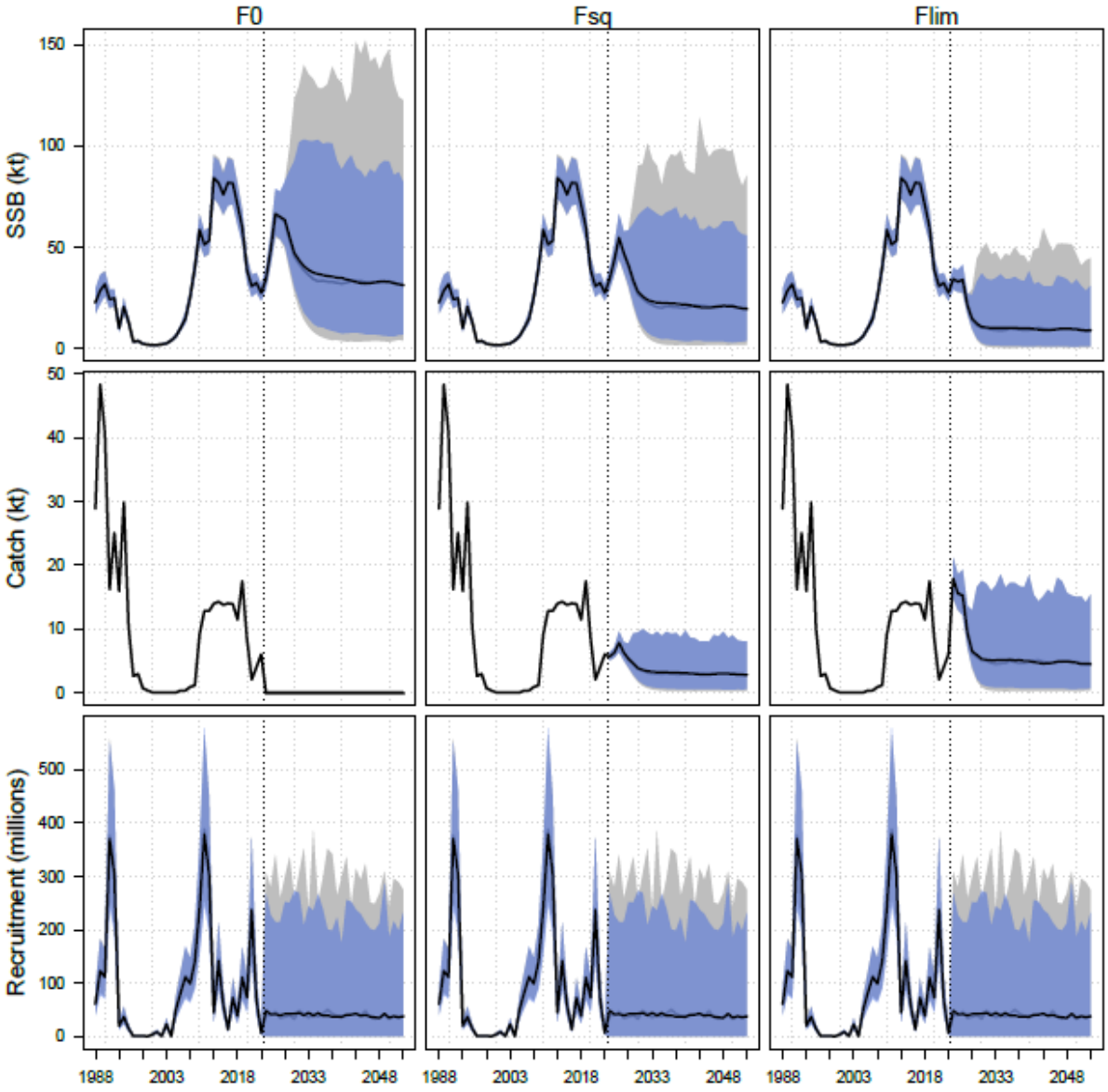

Figure A.7. Comparison of simulation envelopes for the base model (grey shaded region, grey mean line) and the model fit to the spring bloom timing index with a positive projected trend in the index (blue shaded 95% and black mean lines), showing biomass (top), catch (middle row), and recruitment (bottom) over the model history and projection period under no fishing (F0, left hand column), recent average fishing mortality (Fsquo, middle column), and fishing at the fishing mortality limit reference point (Flim, right hand column). Shaded regions show the central 95% of parameter uncertainty under the bayes posterior in the history, and the central 95% of the simulated model states in the projection.

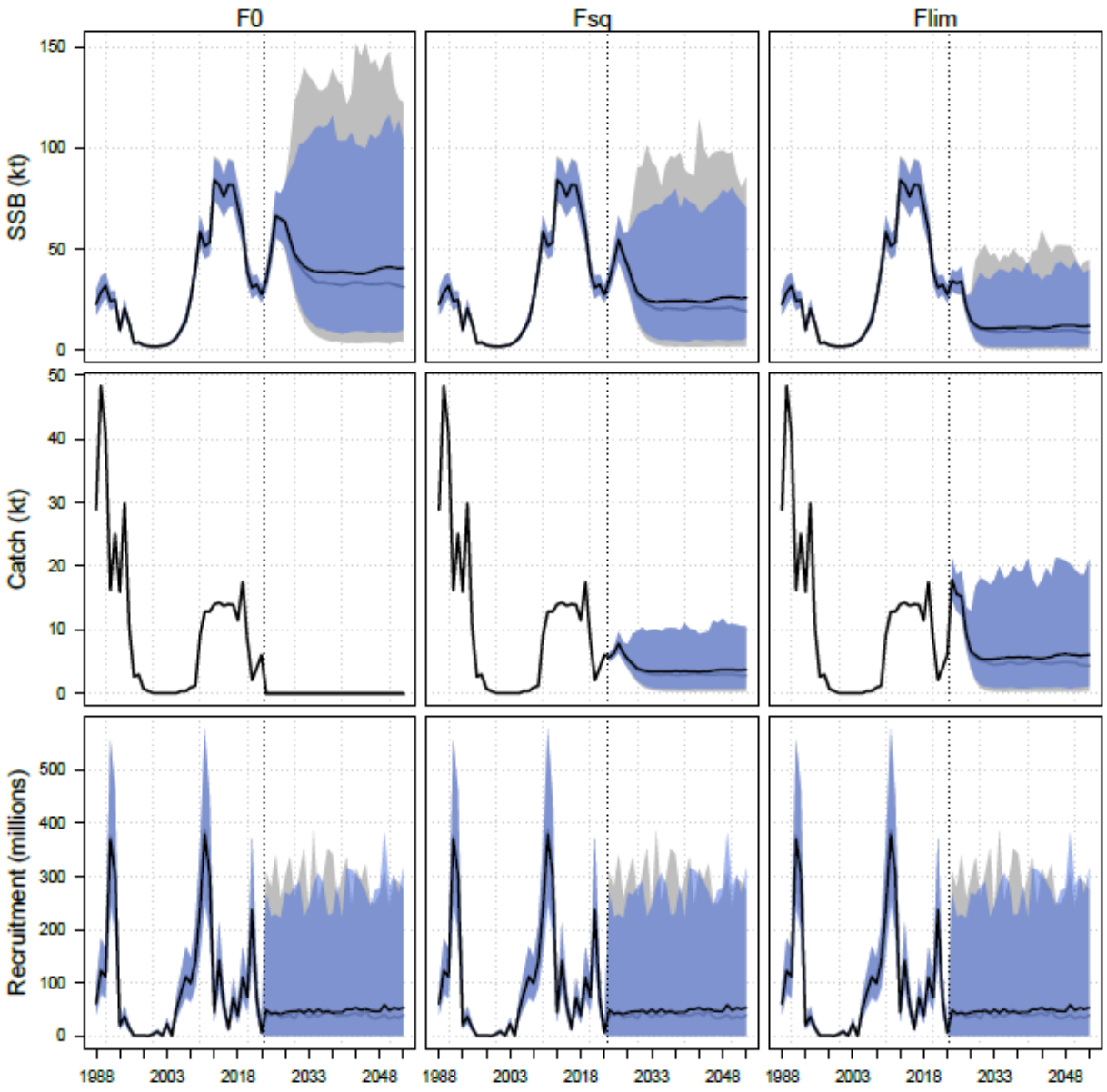

Figure A.8. Comparison of simulation envelopes for the base model (grey shaded region, grey mean line) and the model fit to the spring bloom timing index with a negative projected trend in the index (blue shaded 95% and black mean lines), showing biomass (top), catch (middle row), and recruitment (bottom) over the model history and projection period under no fishing (F0, left hand column), recent average fishing mortality (Fsquo, middle column), and fishing at the fishing mortality limit reference point (Flim, right hand column). Shaded regions show the central 95% of parameter uncertainty under the bayes posterior in the history, and the central 95% of the simulated model states in the projection.

A.2.2 3NO Witch Flounder

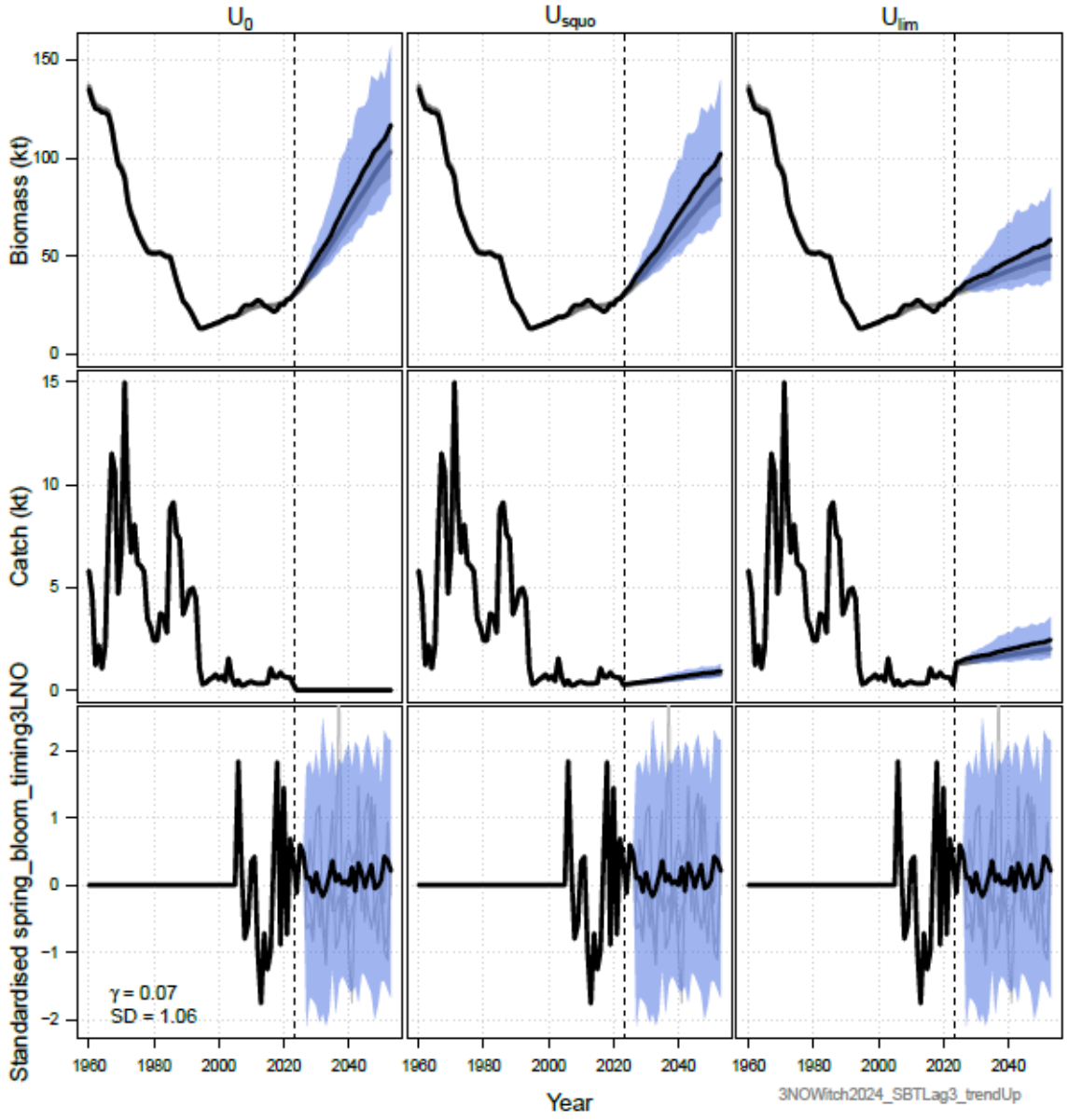

Figure A.9. Spring Bloom timing at lag 3, positive projected trend model simulation envelopes (blue) showing biomass (top), catch (middle row), and standardized Spring Bloom timing (bottom) over the model history and projection period under no fishing (F0, left hand column), recent average fishing mortality (Fsquo, middle column), and fishing at the fishing mortality limit reference point (Flim, right hand column). Shaded regions show the central 95% of parameter uncertainty under the bayes posterior in the history, and the central 95% of the simulated model states in the projection. Light gray lines and regions show the base model. γ is the autocorrelation coefficient of the environmental index. SD is the standard deviation of the difference between successive environmental index values.

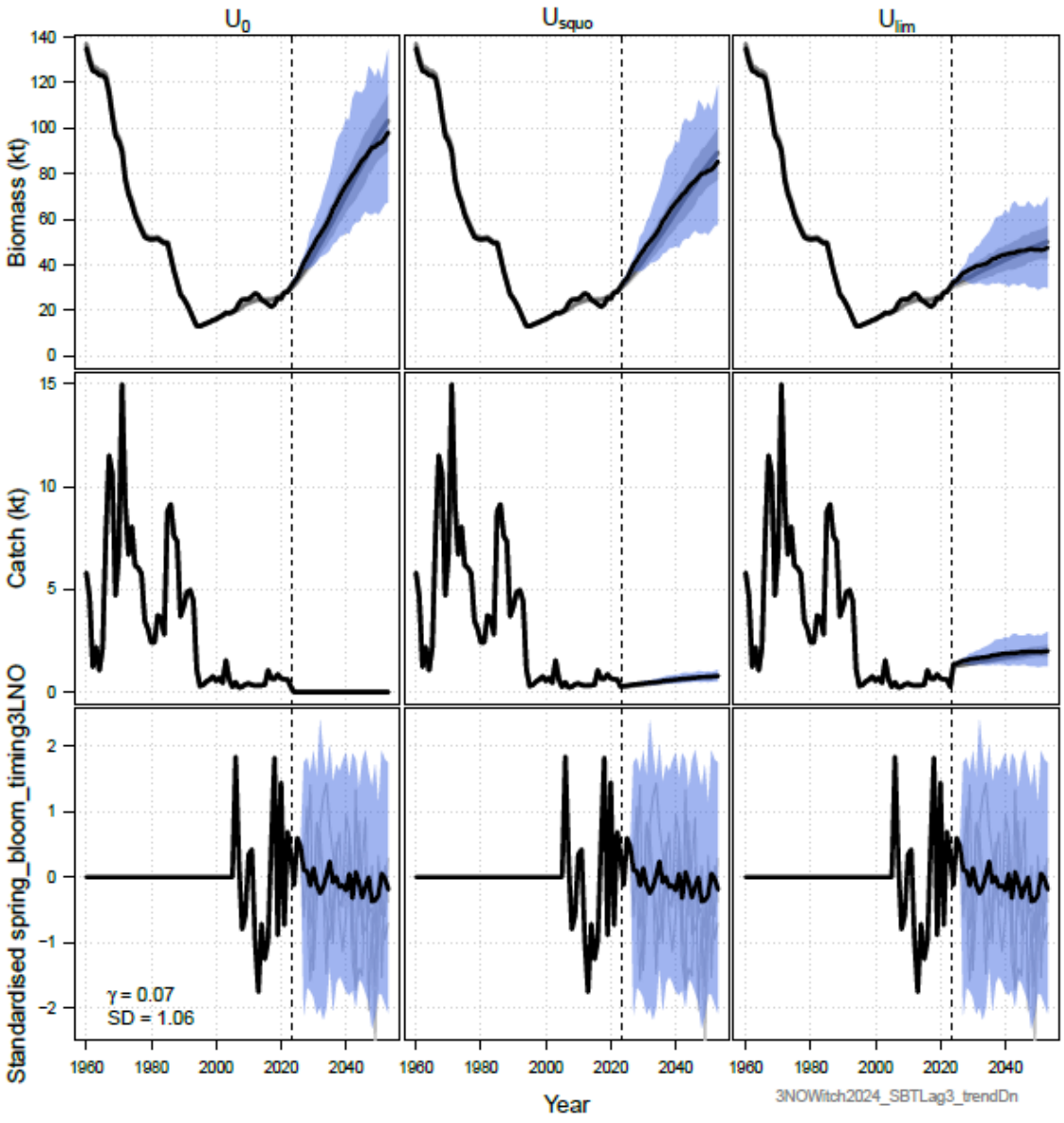

Figure A.10. Spring Bloom timing at lag 3, negative projected trend model simulation envelopes (blue) showing biomass (top), catch (middle row), and standardized Spring Bloom timing (bottom) over the model history and projection period under no fishing (F0, left hand column), recent average fishing mortality (Fsquo, middle column), and fishing at the fishing mortality limit reference point (Flim, right hand column). Shaded regions show the central 95% of parameter uncertainty under the bayes posterior in the history, and the central 95% of the simulated model states in the projection. Light gray lines and regions show the base model. γ is the autocorrelation coefficient of the environmental index. SD is the standard deviation of the difference between successive environmental index values.

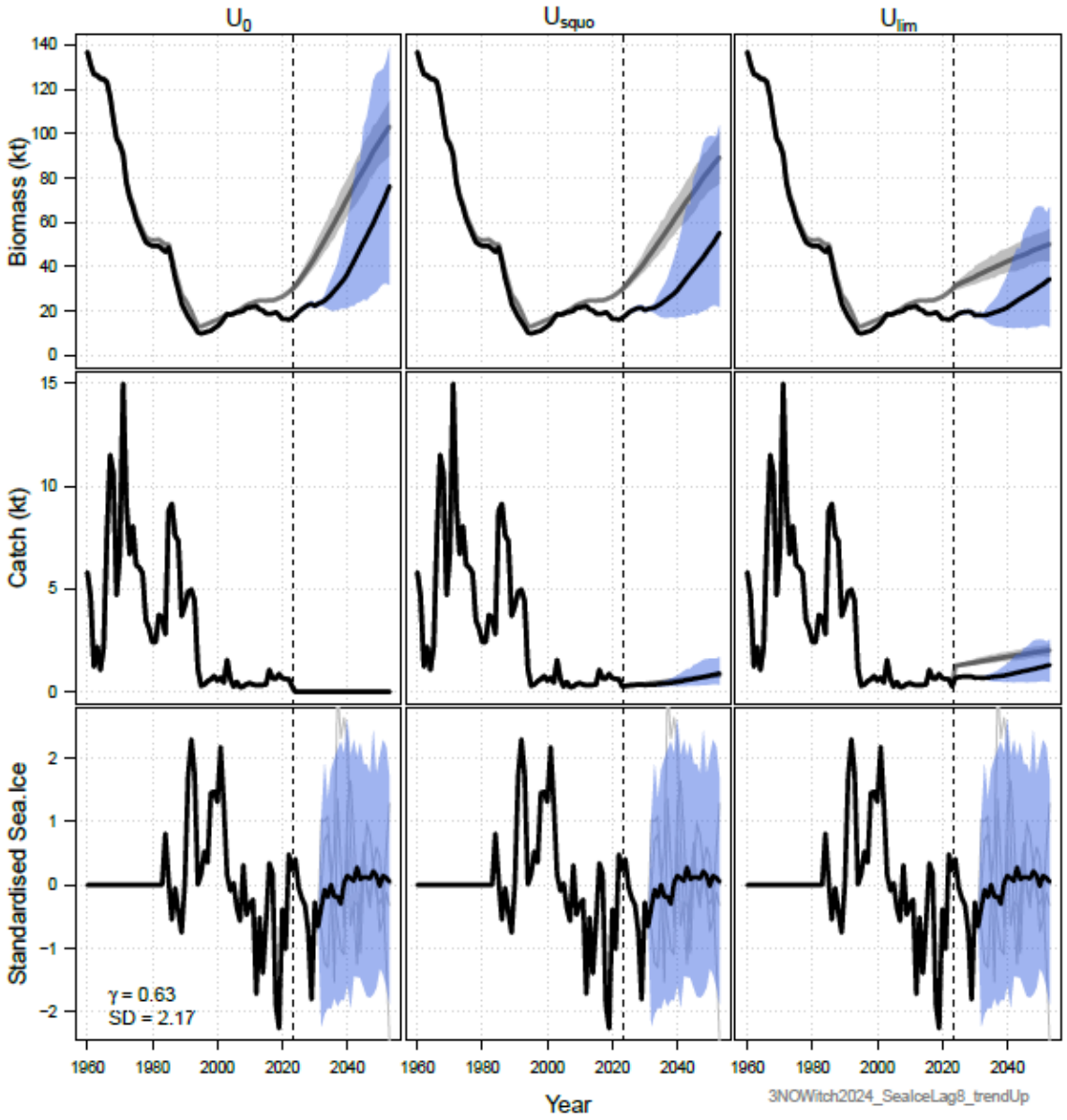

Figure A.11. Sea Ice at lag 8, positive projected trend model simulation envelopes (blue) showing biomass (top), catch (middle row), and standardized Sea Ice (bottom) over the model history and projection period under no fishing (F0, left hand column), recent average fishing mortality (Fsquo, middle column), and fishing at the fishing mortality limit reference point (Flim, right hand column). Shaded regions show the central 95% of parameter uncertainty under the bayes posterior in the history, and the central 95% of the simulated model states in the projection. Light gray lines and regions show the base model. γ is the autocorrelation coefficient of the environmental index. SD is the standard deviation of the difference between successive environmental index values.

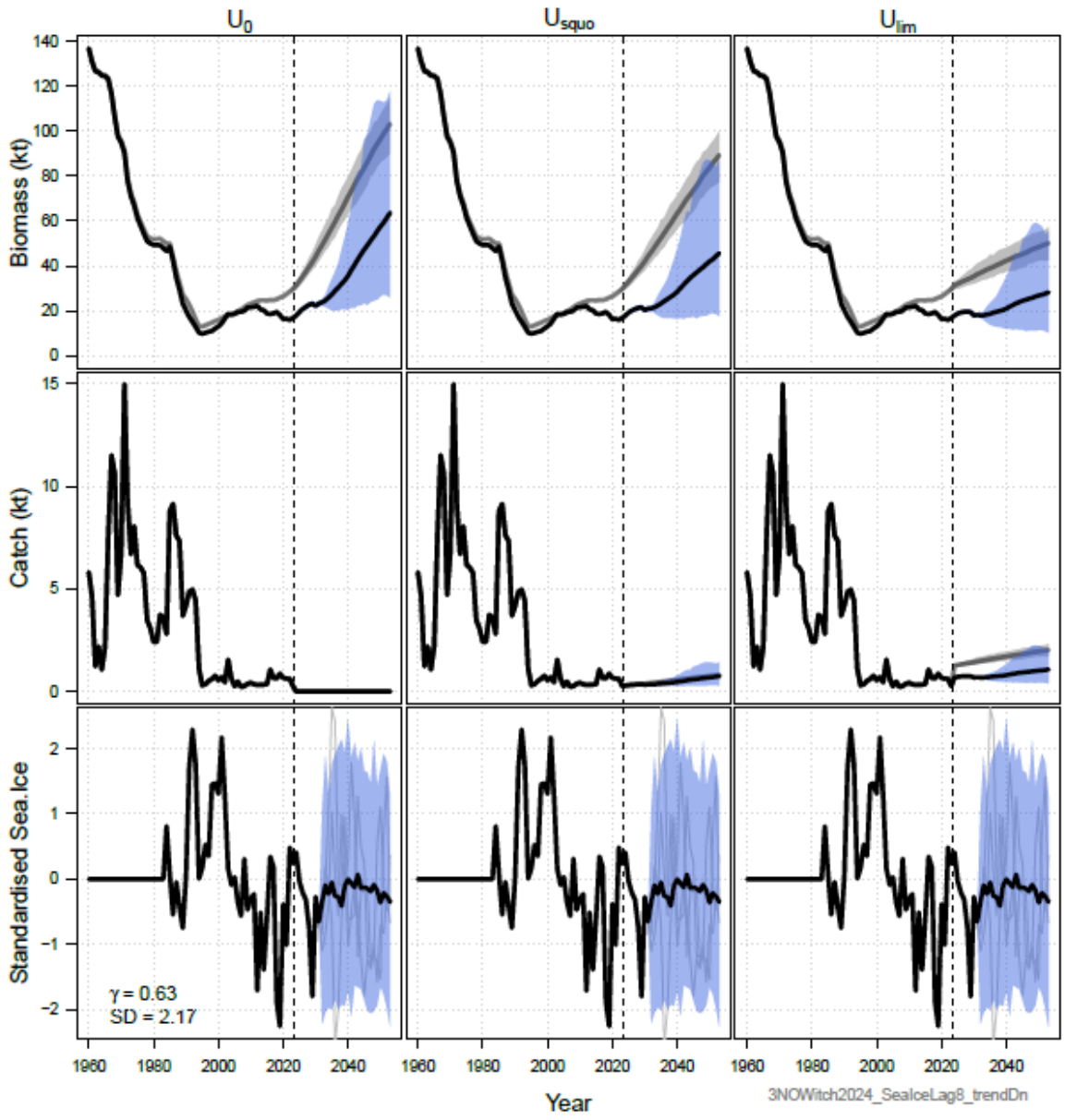

Figure A.12. Sea Ice at lag 8, negative projected trend model simulation envelopes (blue) showing biomass (top), catch (middle row), and standardized Sea Ice (bottom) over the model history and projection period under no fishing (F0, left hand column), recent average fishing mortality (Fsquo, middle column), and fishing at the fishing mortality limit reference point (Flim, right hand column). Shaded regions show the central 95% of parameter uncertainty under the bayes posterior in the history, and the central 95% of the simulated model states in the projection. Light gray lines and regions show the base model. γ is the autocorrelation coefficient of the environmental index. SD is the standard deviation of the difference between successive environmental index values.